GA-A14857
UC-77

PRELIMINARY STRUCTURAL ANALYSIS OF PCRV FOR 300-MW(e) GAS COOLED FAST BREEDER REACTOR

by
G. YOUNG and K. C. CHEUNG

Prepared under
Contract EY-76-C-03-0167
Project Agreement No. 23
for the San Francisco Operations Office
Department of Energy

GENERAL ATOMIC PROJECT 3228
DATE PUBLISHED: MAY 1978

GENERAL ATOMIC COMPANY

ABSTRACT

Preliminary elastic and thermal stress analyses were performed for the multicavity PCRV for the GCFR 300-MW(e) Nuclear Steam Supply System using three-dimensional finite-element computer codes. This report includes information on the finite-element model, material properties, and boundary and loading combinations and presents stress results, evaluations, and recommendations.

In general, the stress levels were found to be acceptable. The stress levels in the concrete ligaments indicate that the existing PCRV configuration can be optimized by increasing the inner ligament and decreasing the outer ligament. For a more exacting optimization of the ligaments, use of a value of effective modulus of elasticity lower than 0.5 E_c in the thermal stress analysis should be justified. The two potential problem areas of the PCRV, the cross-duct region and the bottom head, should be further investigated by local analyses.

The thermal stress analysis indicated that for normal operating conditions it is feasible to eliminate the peripheral tendons.

CONTENTS

FIGURES

TABLE

1. INTRODUCTION

The nuclear steam supply system (NSSS) for the 300-MW(e) Gas Cooled Fast Breeder Reactor (GCFR) comprises the reactor core assembly, a three-loop primary helium cooling system, and a three-loop core auxiliary cooling system. These systems are contained within a prestressed concrete reactor vessel (PCRV) as shown in Fig. 1.*

The PCRV is a multicavity, thick-walled cylindrical structure of high-strength concrete reinforced with bonded reinforcing steel. In order to resist a high internal pressure under operating conditions, the PCRV is prestressed vertically by linear steel tendons and radially by circumferential wire windings.

The design of the PCRV is governed by the ASME Boiler and Pressure Vessel Code, Section III, Division 2 (Ref. 1). Stresses at any location within the concrete vessel must not exceed the allowable values specified in this code under all postulated loading conditions, which include the effects of dead load, prestressing, pressure, temperature, and concrete creep and shrinkage.

A preliminary structural analysis of the reference design PCRV (Ref. 2) for the GCFR Demonstration Plant (Ref. 3) has been performed with the following objectives:

1. Establish acceptable circumferential prestress levels along the height of the vessel.

2. Study the effect of peripheral tendons which are normally provided in the design to accommodate the effect of temperature.

*Figures appear at the end of the text.

3. Confirm that the calculated stresses meet the code allowable values.

Details of the analysis and its results are presented in this report. The PCRV for which the analysis was performed is shown in Figs. 2 and 3.

2. ANALYSIS

In order to determine the structural adequacy of the preliminary design of a PCRV, analytical design procedures are used as specified in the ASME Boiler and Pressure Vessel Code. Elastic and thermal stress analyses are performed to establish the preliminary structural adequacy of a conceptual PCRV. In the elastic stress analysis, the stresses caused by dead load, the vertical prestress, the circumferential prestress, and the maximum cavity pressure are individually calculated. The thermal stress analysis calculates the thermal stresses based on the thermal profile for the normal operating temperature effects.

The load combinations which are considered critical in PCRV sizing are given in Section 2.5.

2.1. METHOD OF ANALYSIS

The elastic stress analysis, including temperature effects, is performed at GA by three-dimensional finite-element computer codes. The analytical methods used in the three-dimensional finite-element analysis are described below.

The analysis was performed by three programs. The first program, MESH3A, was used to prepare the nodal point coordinates and element connectivities which define the finite element model. The prepared data were checked by computing key geometrical parameters for each element in addition to generating plots of the mesh.

The main analysis program, THREED (Ref. 4), was used to compute the three-dimensional displacement and stress fields associated with each loading condition described in Section 2.4. Twenty-node isoparametric brick elements

having a quadratic displacement field were used to model the concrete. The steel liner and cross ducts were represented by eight-node isoparametric membrane elements having displacement fields compatible with the brick faces. The volume and surface integrals associated with the brick and membrane elements were evaluated using 27- and 9-point Gauss formulas, respectively. Linear isotropic elastic constitutive models were used for both materials, with plane stress conditions imposed on the membrane elements.

The boundary conditions on the symmetry planes and support were imposed by specifying zero displacement normal to the surface. Pressure forces were computed in the program by determining an energy equivalent set of nodal forces. An algorithm for specifying an arbitrary force at any point was developed and used to model the reaction forces resulting from curved linear prestressing tendons.

A third program, PRINT3, was used to display the results in printed and plotted format for engineering interpretation. This program contains several features which enable the analyst to easily locate regions of the model requiring detailed study.

2.2. ANALYTICAL MODEL

Using the conditions of symmetry, only one-sixth of the PCRV was considered in the three-dimensional finite-element analysis described in this report. The finite-element model is depicted in Figs. 4 and 5. The model represents a 60° sector of the PCRV which is bounded by the vertical planes through the centers of the steam generator cavity and the auxiliary heat exchanger cavity (Figs. 2 and 3). The entire model is first identified by 21 planes as shown in Fig. 4. Each layer between two neighboring planes is then divided into a number of brick elements. Figure 5 illustrates the brick elements identified for a given layer, in this case the layer between planes 20 and 21. The entire model consists of a total of 305 brick elements and 38 membrane elements. The 20-node isoparametric brick elements

were used to model the PCRV concrete while the 8-node membrane elements were used to model the steel penetration liners. For simplicity only the major cavities, namely, the reactor core cavity, the steam generator cavities, the auxiliary circulator cavity, and the cross ducts, were modeled.

The prestressing and reinforcing steels were not included in the model. However, the prestressing forces were treated as external loads as described in Section 2.4. The configuration and dimensions of the finite-element model were based on Ref. 2. Major dimensions of the PCRV are shown in Fig. 2.

2.3. PROPERTIES OF MATERIALS

The following material properties were used in the analysis:

Concrete

Compressive strength at 60 days (f'_c) = 44.8 MPa (6500 psi)
Modulus of elasticity (E_c) = 39.989×10^3 MPa (5.8×10^6 psi)
Poisson's ratio = 0.2
Linear coefficient of thermal expansion = 10.8×10^{-6}/°C (6.0×10^{-6}/°F)
Tensile strength (F_{ct}) = $0.623 \sqrt{f'_c}$ MPa where f'_c is in MPa
= $7.5 \sqrt{f'_c}$ psi where f'_c is in psi

Steel Penetration Liner

Modulus of elasticity (E) = 186.159×10^3 MPa (27×10^6 psi)
Poisson's ratio = 0.3
Linear coefficient of thermal expansion = 11.7×10^{-6}/°C (6.5×10^{-6}/°F)
Liner thickness for refueling penetration = 25.4 mm (1 in.)
Liner thickness for lower steam generator penetration = 19.1 mm (3/4 in.)

2.4. LOADING CONDITIONS

The loadings considered in the elastic stress analysis were prestressing forces due to the linear prestressing system (LPS), prestressing forces due to the circumferential prestressing system (CPS), and the maximum cavity pressure (MCP). The effect of normal operating temperatures (T_o) was included in the loading conditions for the thermal stress analysis.

2.4.1. Linear Prestressing System (LPS)

Prestressing forces due to the LPS were treated as concentrated loads, generally vertical, applied at the top and bottom surfaces of the PCRV. The horizontal components of the tendon forces associated with the local curvature of tendons were evaluated and applied at appropriate locations as part of the loading. Friction forces along the tendons were considered negligible.

Locations of tendons used in the analyses are shown in Fig. 6, with these locations deviating from those shown in Fig. 3 to the extent that the tendons between the steam generator cavity and the core auxiliary circulator cavity were rearranged along the cross ducts. The total number of tendons remained the same.

The magnitude of the concentrated load for each tendon was computed as follows:

Guaranteed ultimate tensile strength (GUTS) for the material ASTM A421, Gd 240 = 1654.7 MPa (240 ksi).

GUTS for each tendon of 170 wires of 6.4 mm (1/4 in.) diameter = 888.8×10^3 N (2000 kips).

Initial prestress force for each tendon = 0.7 GUTS = 622.2×10^3 N (1400 kips).

Prestress force at end of vessel design life = 82% of the initial prestress force = 506.6 x 10^3 N (1140 kips).

The effect of the peripheral tendons on the ligament stresses in the PCRV was separately investigated. As shown in Fig. 3, 75 vertical tendons are located at the periphery of the PCRV. These peripheral tendons are included to counteract the vertical tensile stresses in the outer ligament resulting from thermal gradients in the wall and are not essential to maintaining the structural integrity of the PCRV. Thus, the effect of eliminating the peripheral tendons was examined in the thermal analysis; the results are reported in Section 3.

2.4.2. Circumferential Prestressing System (CPS)

For the elastic analysis the prestressing forces provided by the wire winding of the CPS were treated as bands of uniform radial pressure. The average circumferential prestress levels for the top head, barrel section, and bottom head of the PCRV were considered separately as shown in Fig. 7. A uniform radial pressure of 6.89 MPa (1000 psi) for each region was used for initial computer runs to establish the circumferential prestress requirements. The circumferential prestress was determined using the following data:

GUTS of 12.7 mm (1/2 in.) diameter strand = 183.6 x 10^3 N (41.3 kips).
Average initial prestress per layer of wire = 6875.6 x 10^3 N (1547 kips).
Prestress at end of vessel design life = 80% of initial prestress.

Two circumferential prestress loadings were investigated:

1. CPS Loading A

   Top head

   7.05 MPa (1023 psi)(corresponds to initial prestress provided by 14 layers)

Barrel

6.56 MPa (951 psi)(corresponds to initial prestress provided by 13 layers)

Bottom head

9.07 MPa(1316 psi)(corresponds to initial prestress provided by 18 layers)

2. CPS Loading B

Top head

6.05 MPa (878 psi)(corresponds to initial prestress provided by 12 layers)

Barrel

7.56 MPa (1097 psi)(corresponds to initial prestress provided by 15 layers)

Bottom head

9.07 MPa (1316 psi)(corresponds to initial prestress provided by 15 layers)

In the analyses average uniform circumferential prestress levels in the top head, barrel section, and bottom head of the PCRV were used. A more effective use of the circumferential prestress would be to vary the prestress level at appropriate locations to obtain the desired stress distributions in the PCRV. Detailed analyses were performed to determine the number of layers of strands required for each of the prestressing channels. A description of the results is given in Section 3.

2.4.3. Maximum Cavity Pressure (MCP)

All cavities and penetrations included in the finite-element model were loaded with the MCP of 10.19 MPa (1478 psi). Cavity closure and

penetration loads were input as a series of concentrated loads at the positions of the shear anchors.

The MCP is derived from the normal working pressure (NWP) by:

NWP = 8.99 MPa (1305 psi)
Design Pressure (DP) = NWP x 1.1 = 9.90 MPa (1436 psi)
MCP = DP x 1.03 = 10.19 MPa (1478 psi)

2.4.4. Thermal Loading

A steady-state thermal analysis was performed using the thermal boundary conditions given in Ref. 5. The temperature distributions from the thermal analysis were used to determine the thermal stresses described in Section 3. An effective modulus of elasticity equal to 0.5 E_c was used.

2.5. LOADING COMBINATIONS

The GCFR PCRV has been designed to meet the requirements of the ASME Code (Ref. 1), which states that the pressure vessel shall be designed for service conditions stipulated in the Design Specifications by maintaining the levels of stress, strain, and deformations to limits that ensure an essentially elastic response under normal service life of the vessel.

The stress strength limits specified in the ASME Code for primary stress and for primary stress plus secondary stress must be met for all the loading combinations. Based on GA experience, the following load combinations were considered critical in PCRV sizing:

1. DL + F_i (for maximum compressive stresses)
2. DL + F_t + T_o + MCP (for maximum tensile stresses)

where DL = dead loads including vessel weight, all pertinent equipment weight, and piping loads,

F_i = initial prestress,

F_t = prestress at time of consideration,

T_o = normal operating temperature including normal startup and shutdown,

MCP = all loads due to maximum cavity pressure.

The dead load effect on the overall PCRV stresses was considered insignificant and was ignored. In the preliminary analysis to establish the maximum compressive stress, the initial prestress loading was used. To establish the maximum tensile stresses present in the ligaments, the load case at end-of-life prestress and the MCP were used with the effects of the normal operating temperature (F_e + MCP + T_o).

3. RESULTS OF ANALYSIS

Stress plots of the critical loading combinations were prepared for representative sections of the PCRV. Only the critical components of the concrete ligament stresses were plotted. Stresses were determined at the integration points of the finite element closest to the section under consideration. Key locations of the stress plots are given in Fig. 8. A tabulation of normal stresses at key locations derived from the stress plots is given in Table 1.

An investigation was conducted to compare the stresses resulting from the use of various CPS loadings as described in Section 2.4.2. It was found that improved stress distributions in the barrel were obtained from loading combinations combined with the CPS loading B. The investigation was continued to obtain a more effective use of the circumferential prestress by varying the prestress level at appropriate locations to obtain the desired stress distributions in the PCRV. The resulting number of layers of the circumferential prestressing strands in each channel on the basis of 22 channels for the entire PCRV is shown in Fig. 9.

The effects of the peripheral tendons on ligament stress for the loading conditions using the mechanical and thermal loading combinations (F_e + MCP + T_o) are presented in Figs. 10 through 16. Figures 10 through 12 show the axial and hoop stresses in the section through the core and steam generator cavities midway between the cross ducts. The stress distributions in ligaments at midheight of the PCRV barrel section (Z = 703) are shown in Figs. 13 through 16.

It can be seen that the peripheral tendons have an insignificant effect on the hoop stresses in the barrel. The peripheral tendons did provide an additional axial compressive stress of the magnitude of 1.03 to 1.38 MPa (150 to 200 psi) in the outer ligament. Without the peripheral tendons, the average stresses in the ligament still remain within the ASME Code allowable

TABLE 1
KEY LOCATION STRESSES

Load Combination	1[a]		2		Average		3		4		Average		5		6		Average	
	σ_r[b]	σ_θ	σ_r	σ_θ	σ_r	σ_θ	σ_r	σ_θ	σ_r	σ_θ	σ_r	σ_θ	σ_r	σ_θ	σ_r	σ_θ	σ_r	σ_θ
F_i	-2400	-	-1760	-	-1360	-	+80	-2700	-620	-4360	-820	-3420	-650	-3830	-780	-1800	-960	-2560
$F_e + MCP + T_o$	+520	-	+510	-	+360	-	+50	+240	+220	+440	-380	-110	+120	-620	-700	-160	-640	-60
	7		8		Average		9		10		Average		11		12		Average	
	σ_r	σ_θ	σ_r	σ_θ	σ_r	σ_θ	σ_r	σ_θ	σ_r	σ_θ	σ_r	σ_θ	σ_r	σ_θ	σ_r	σ_θ	σ_r	σ_θ
F_i	-280	-2320	-240	-2800	-760	-2480	-540	-2440	-880	-1060	-680	-1380	-120	-2880	-320	-3320	-440	-2500
$F_e + MCP + T_o$	-240	+120	+240	+260	-330	+80	+100	+100	-820	-280	-430	-10	-1460	-560	-1380	-240	-1320	-600
	13		14		Average		15		16		Average		17		18		Average	
	σ_r	σ_θ	σ_r	σ_θ	σ_r	σ_θ	σ_r	σ_θ	σ_r	σ_θ	σ_r	σ_θ	σ_r	σ_θ	σ_r	σ_θ	σ_r	σ_θ
F_i	-450	-3100	-1360	-1940	-980	-2180	-120	-2280	-1320	-1300	-900	-1480	-320	-1540	-410	-1960	-1340	-1350
$F_e + MCP + T_o$	-1460	-200	-1080	+40	-1180	-160	-1480	-1020	-1090	-600	-1140	-790	+200	-40	-700	+100	-890	-320
	19		20		Average		21		22		Average		23		24		Average	
	σ_r	σ_θ	σ_r	σ_θ	σ_r	σ_θ	σ_r	σ_θ	σ_r	σ_θ	σ_r	σ_θ	σ_r	σ_θ	σ_r	σ_θ	σ_r	σ_θ
F_i	-690	-2020	-600	-2040	-860	-1430	-460	-1980	-1020	-1460	-1310	-1700	-300	-1480	-940	-870	-660	-1090
$F_e + MCP + T_o$	-740	+250	-610	+370	-375	+120	-880	0	-890	-230	-1220	-380	+160	-140	+260	-140	+175	-110
	25		26		Average													
	σ_r	σ_θ	σ_r	σ_θ	σ_r	σ_θ												
F_i	-970	-660	-1390	-1460	-1380	-1220												
$F_e + MCP + T_o$	+10	-60	-1080	-940	-790	-680												

[a] Numbers 1 through 26 are key locations (from Fig. 8).

[b] σ is stress in psi (1 psi = 6.9×10^{-3} MPa).

values. In the case where the peripheral tendons are omitted, as shown in Fig. 10, the axial tensile stress exceeds the ASME "point stress" allowable value but since the affected region is localized, the stress would be considered acceptable according to paragraph CB-3450 of the ASME Code.

Plots of the radial and hoop stresses in the PCRV are presented in Figs. 17 through 42. The loading combinations used are those given in Section 2.5 for finding the maximum compressive stresses by the initial prestress loading (F_i) and the maximum tensile stresses for the loading of end-of-life prestress, the maximum cavity pressure, and the effect of normal operating temperature (F_e + MCP + T_o). The analysis was performed for the prestress condition which includes peripheral tendons and the case of the effective use of circumferential strands in each channel as previously determined. The radial stress distributions between the steam generator and auxiliary circulator cavities are given in Figs. 41 and 42.

4. EVALUATION AND RECOMMENDATIONS

The evaluation of the elastic stress analysis using the mechanical and thermal loading conditions of (F_e + MCP + T_o) indicates that the results show the overall PCRV sizing is adequate. A study of the stresses at normal operating conditions with and without the peripheral tendons shows it would be feasible to eliminate the peripheral tendons; however, to establish that elimination of peripheral tendons is possible for abnormal temperature cases, such cases should be studied in additional analyses.

The stress levels in the concrete ligaments between the steam generator cavity and the reactor core cavity indicate that the PCRV configuration can be improved in future configurations by relocating the steam generator cavity outboard to increase the inner ligament and decrease the outer ligament. Increasing the inner ligament and the ligament between the steam generator and auxiliary loop cavities would also improve stress conditions at the top of the PCRV. In order to optimize the ligament sizes, it is recommended that use of a value of effective modules of elasticity lower than 0.5 E_c be justified in the thermal analysis.

5. POTENTIAL PROBLEM AREAS

Two potential problem areas in the PCRV were identified on the basis of the stress results of the elastic analysis:

1. Refueling penetration region in the bottom head. Initial analysis showed high tensile stresses in the ligament between the refueling penetrations due to full pressurization of the central penetration. The tensile stress level was not sufficiently reduced by the addition of higher circumferential prestress in the bottom head. The problem was resolved by pressurizing only the upper portion of the central refueling penetration to simulate the effect of incorporation of a stress-relief sleeve. In subsequent analysis, 1.3 m (51 in.) of the lower portion of the penetration was not pressurized. It would be beneficial to perform a local three-dimensional analysis for the bottom head to include both refueling and lower steam generator penetrations in the finite-element model.

2. Cross-duct region in upper PCRV. Localized high concrete stresses were found in areas between the upper and lower cross ducts. Apart from effects of stress concentration, the high stresses were attributed to the inadequate finite-element representation of the cross-duct region. Detailed local three-dimensional analysis is required to accurately predict the state of stress in this region.

6. ADDITIONAL ANALYSES

Additional analyses which should be performed on the PCRV to finalize the design include:

1. Local three-dimensional analysis of the top head. The finite-element model should include detailed representation of the crossducts and closure shear anchor loads. Cavity and crossduct liners should be incorporated to determine compressive strains for liner design.

2. Local three-dimensional analysis of the bottom head and lower steam generator closure. A single finite-element model can be used for both the bottom head and the lower steam generator region. It would be advisable to include in the model the PCRV support structure to determine the effect of circumferential prestress in the PCRV. To determine the structural adequacy of the bottom head, supplementary ultimate load analyses should be undertaken.

3. Three-dimensional analysis for the effects of abnormal temperatures to establish if the peripheral tendons can be eliminated.

7. REFERENCES

1. ASME Boiler and Pressure Vessel Code, Section III, Division 2, "Code for Concrete Reactor Vessels and Containments, Nuclear Power Plant Components."
2. General Atomic Drawing 1304-0285, Sheet 1, "PCRV, Vertical Section," and Sheet 2, "PCRV, Plan View," unpublished data.
3. "Development Plans for Gas-Cooled Fast Breeder Reactor (GCFR) Nuclear Steam Supply (NSS) Components," General Atomic Report GA-A14462, September 1977.
4. Young, R., "Program THREED Input Reference Manual," General Atomic unpublished data, January 1975.
5. Jovanovic, V., "300-MW(e) GCFR PCRV Thermal Boundary Conditions for Steady-State Normal Operating Conditions - Update," General Atomic unpublished data, September 24, 1976.

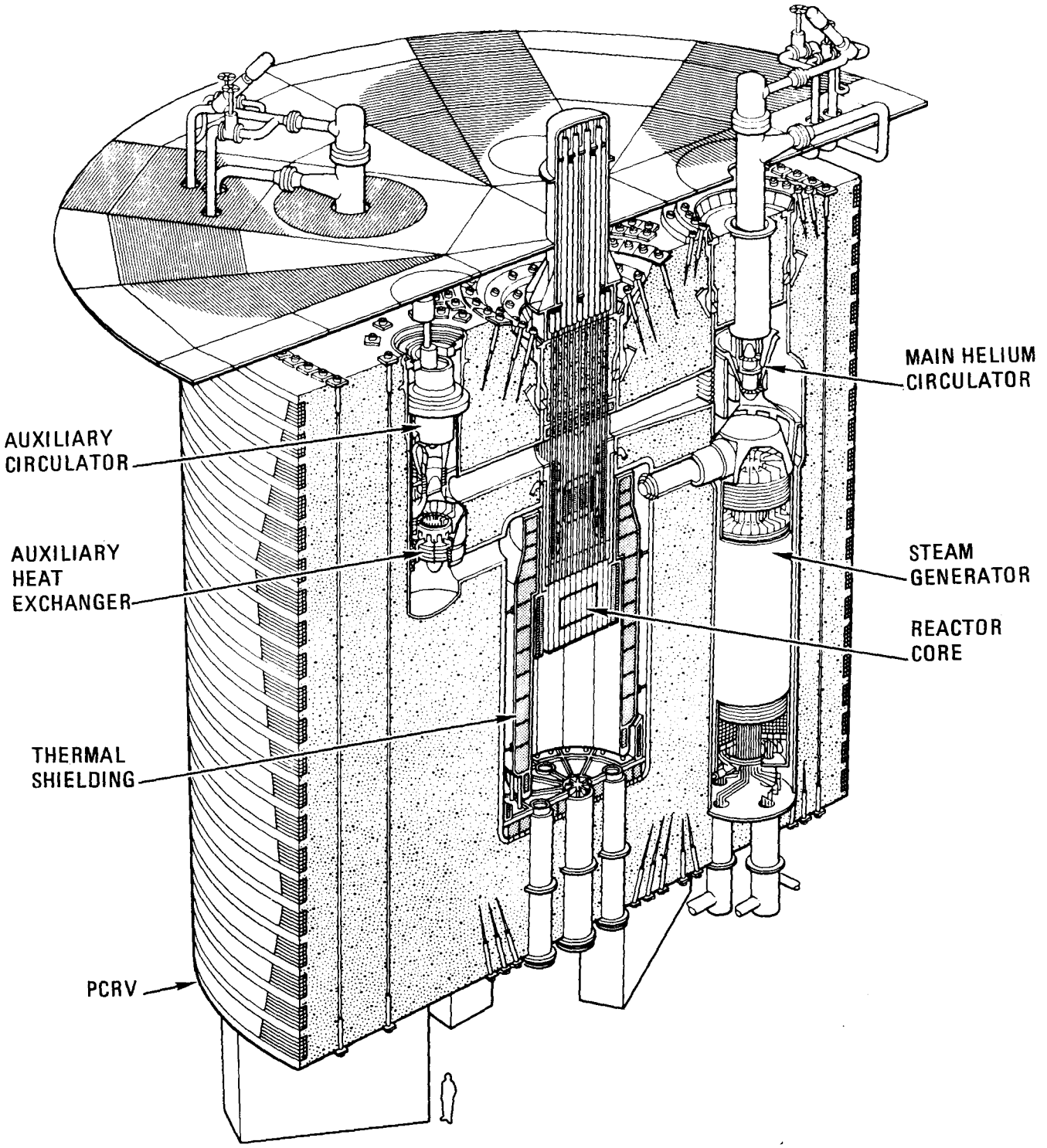

Fig. 1. Nuclear Steam Supply System for 300-MW(e) GCFR

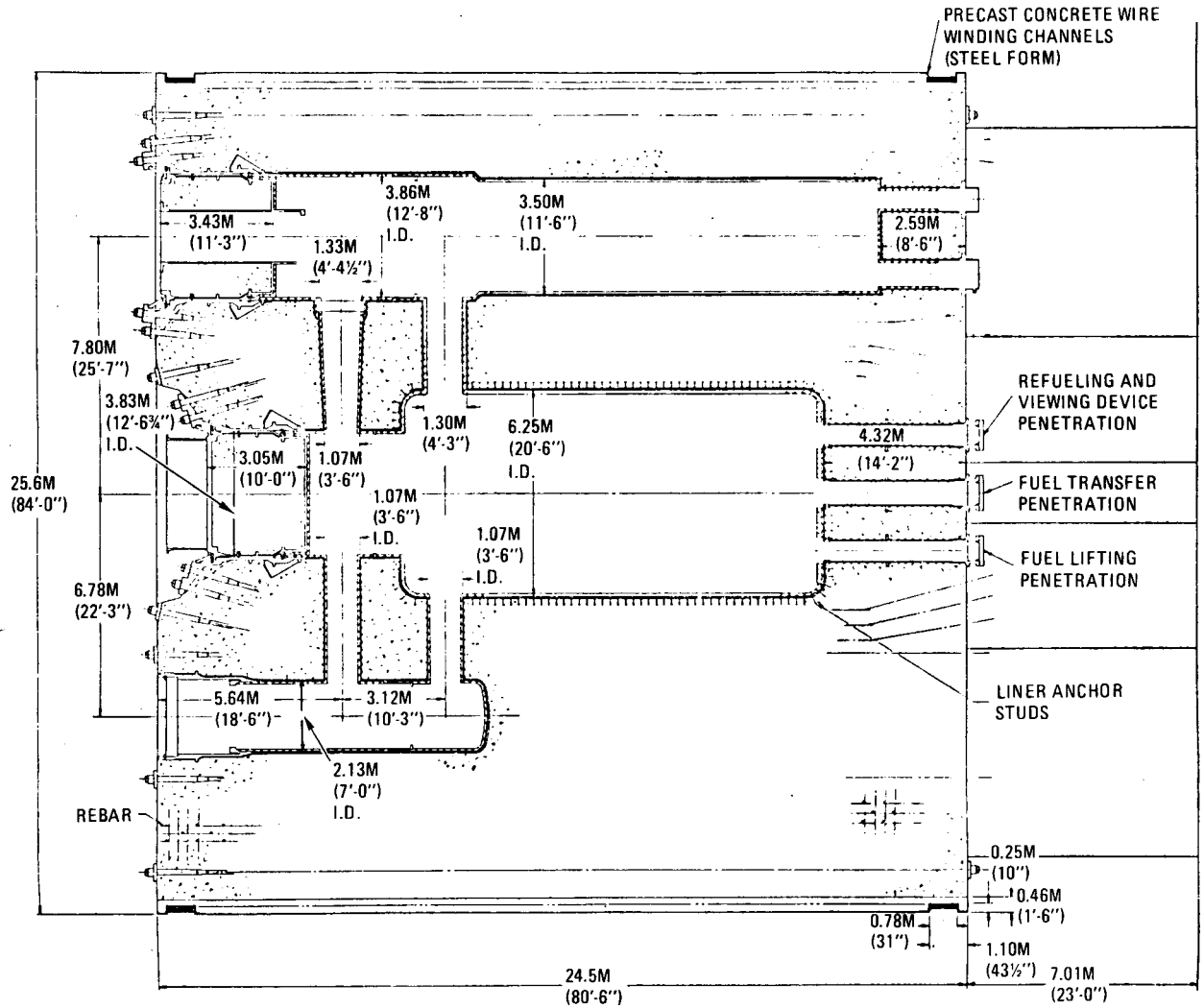

Fig. 2. PCRV vertical section

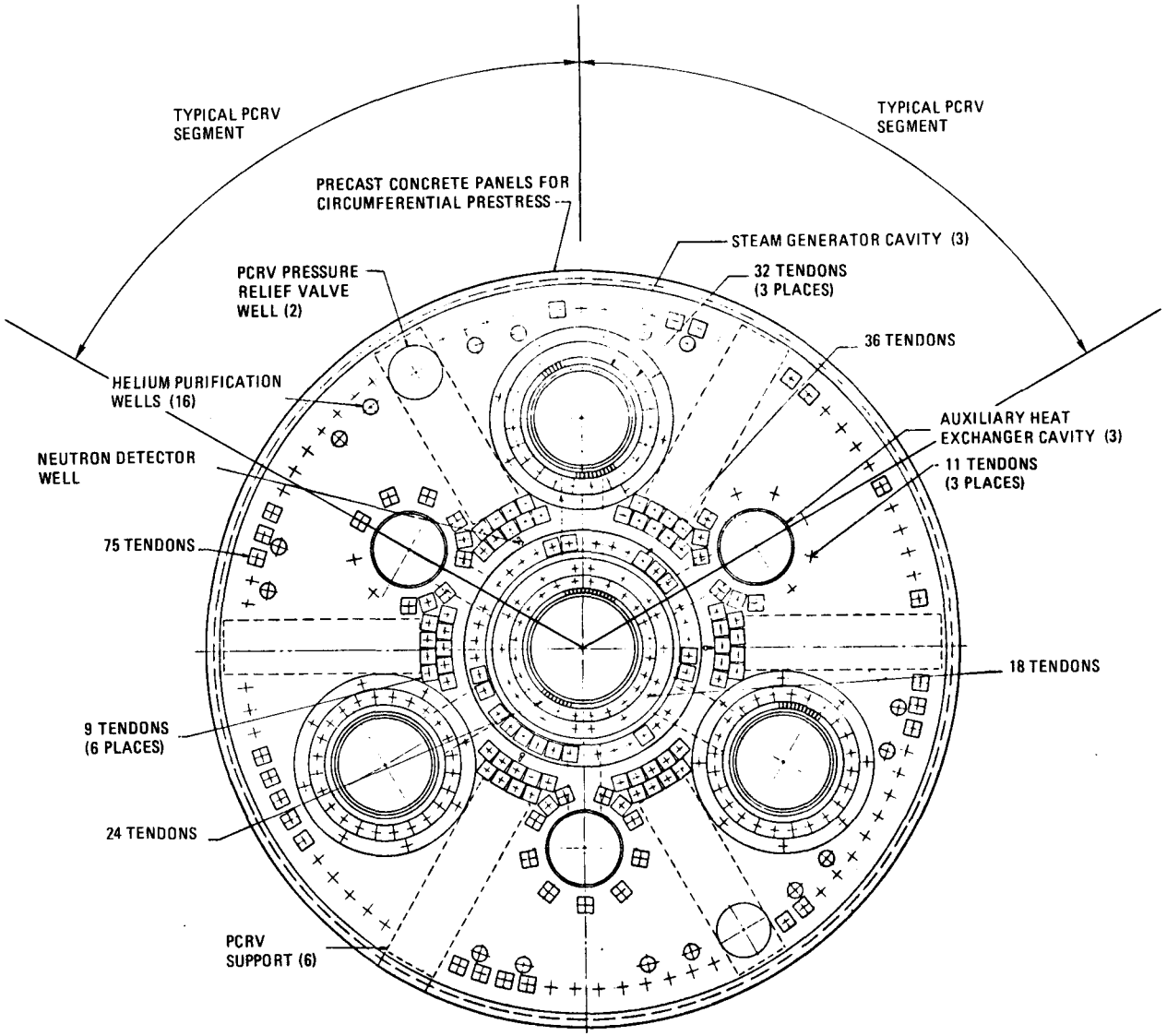

Fig. 3. PCRV plan view (top head)

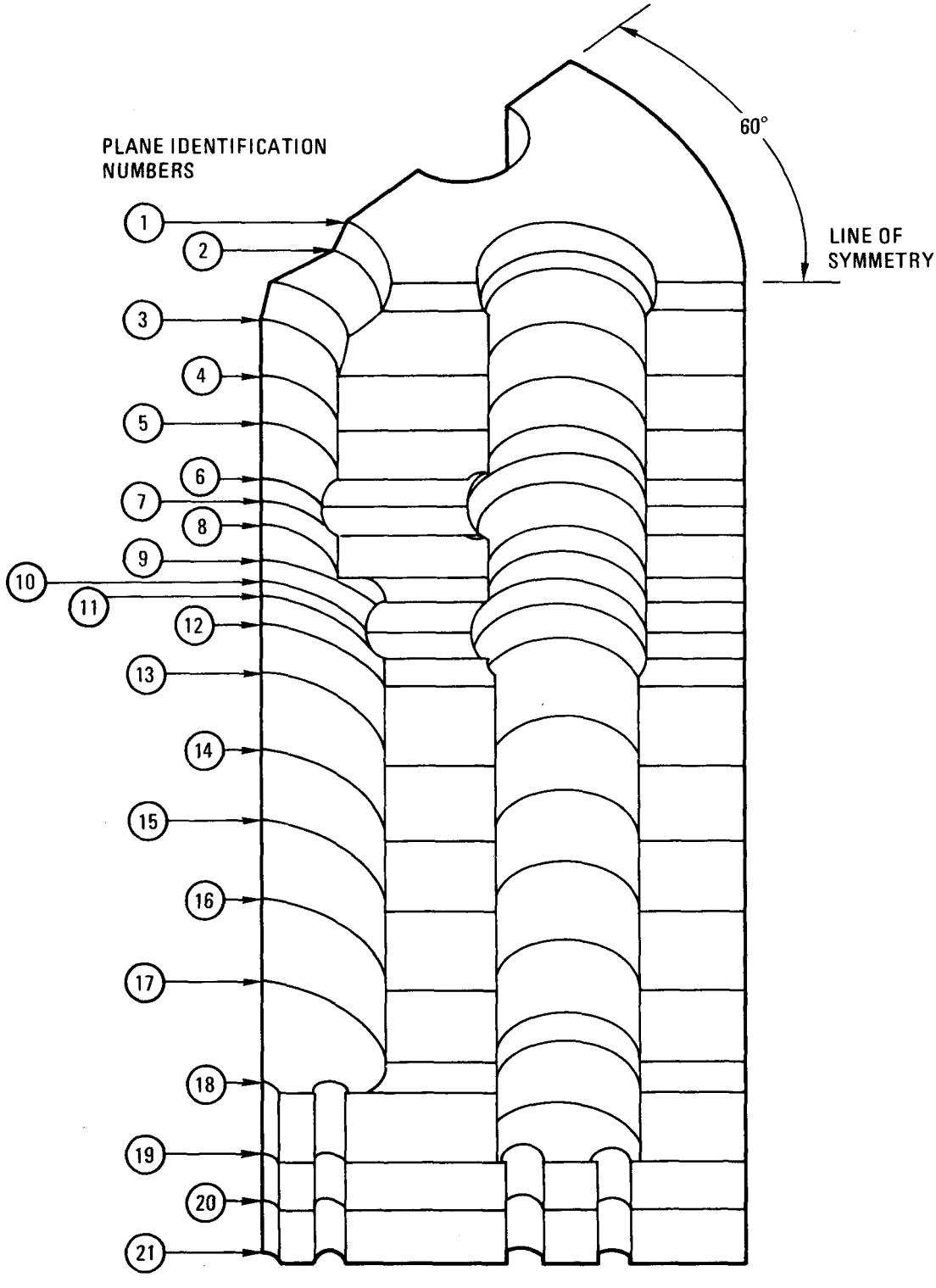

Fig. 4. Finite-element model

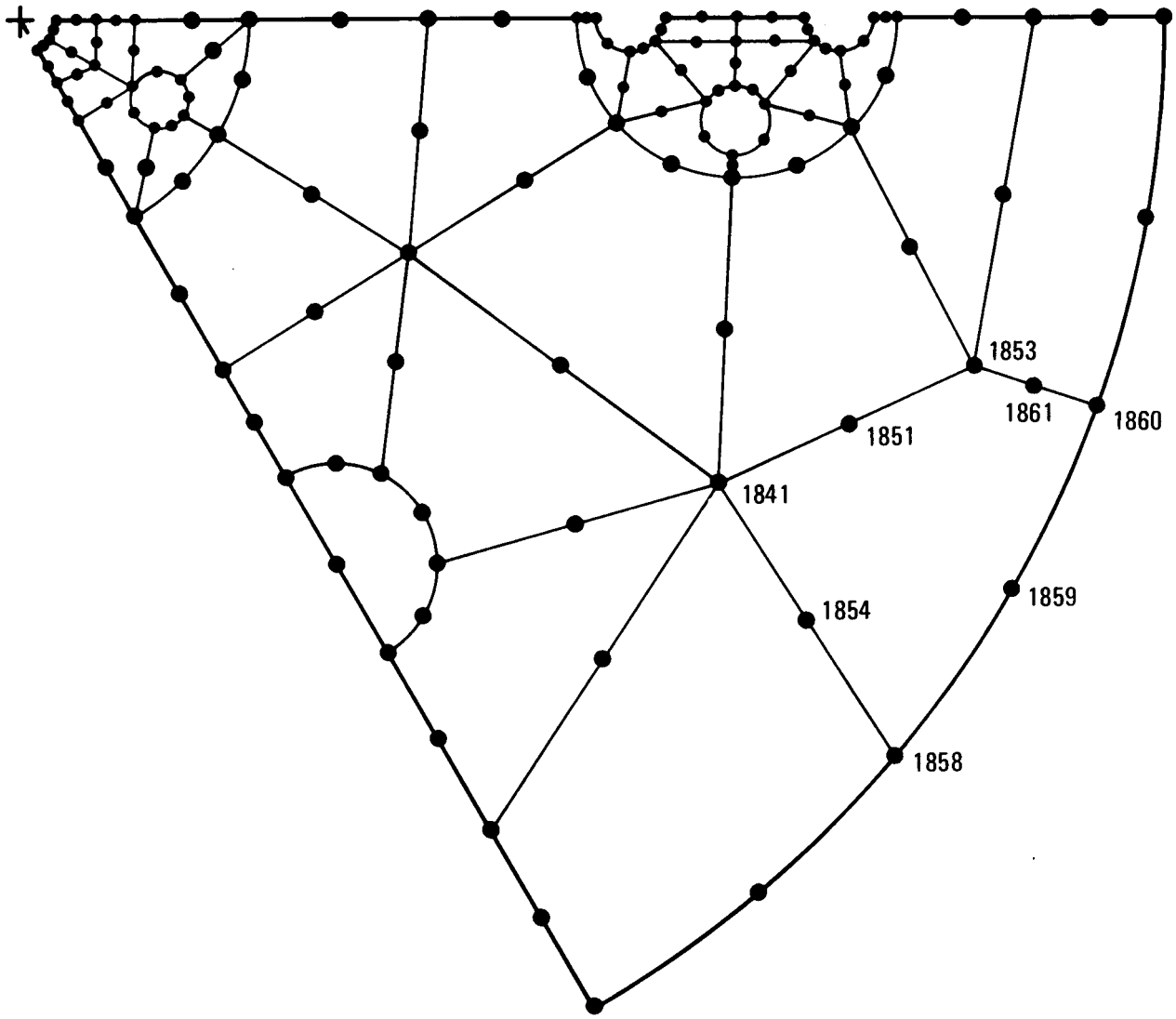

Fig. 5. Brick elements: (a) plane 20

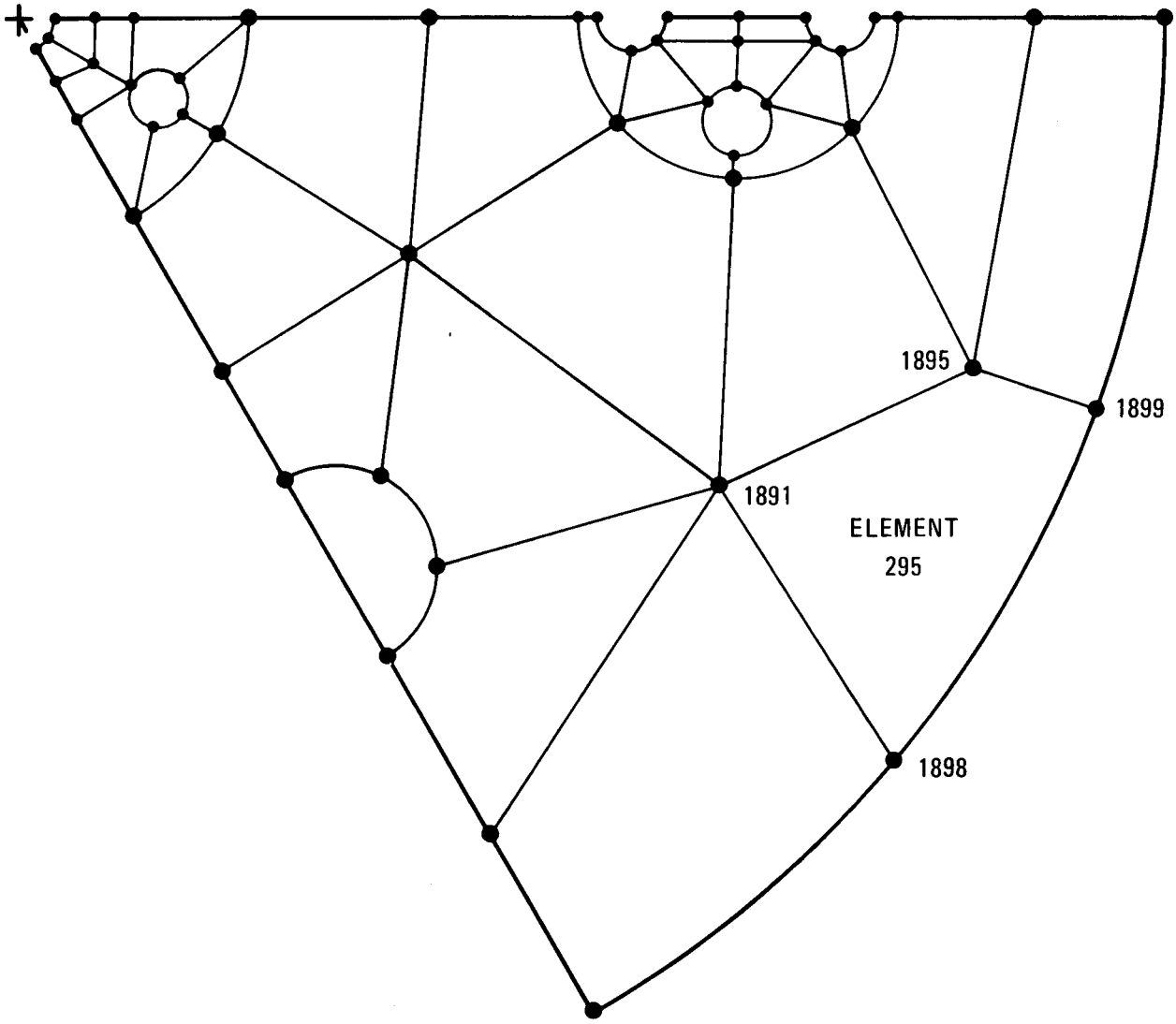

Fig. 5. Brick elements: (b) planes 20 and 21

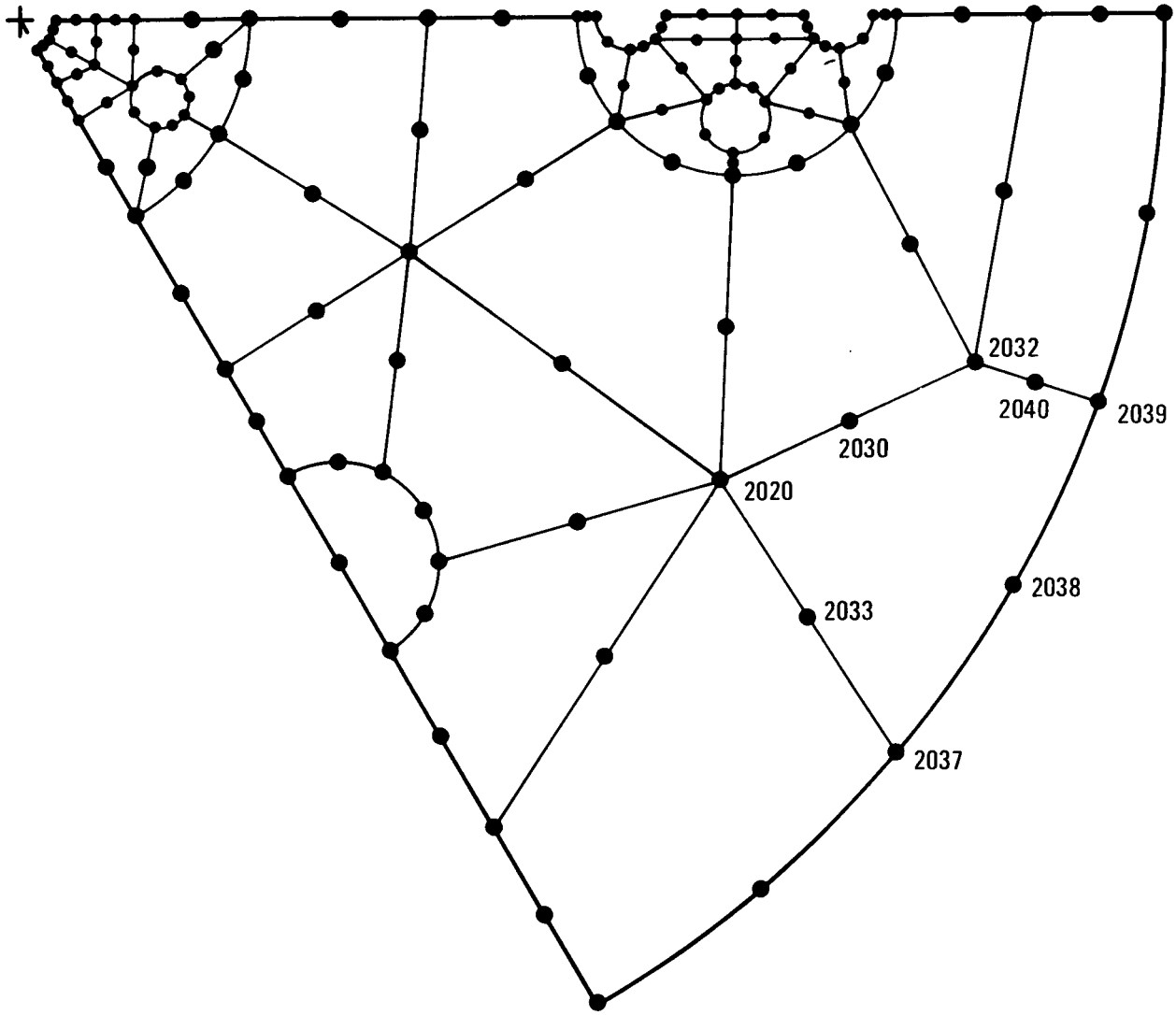

Fig. 5. Brick elements: (c) plane 21

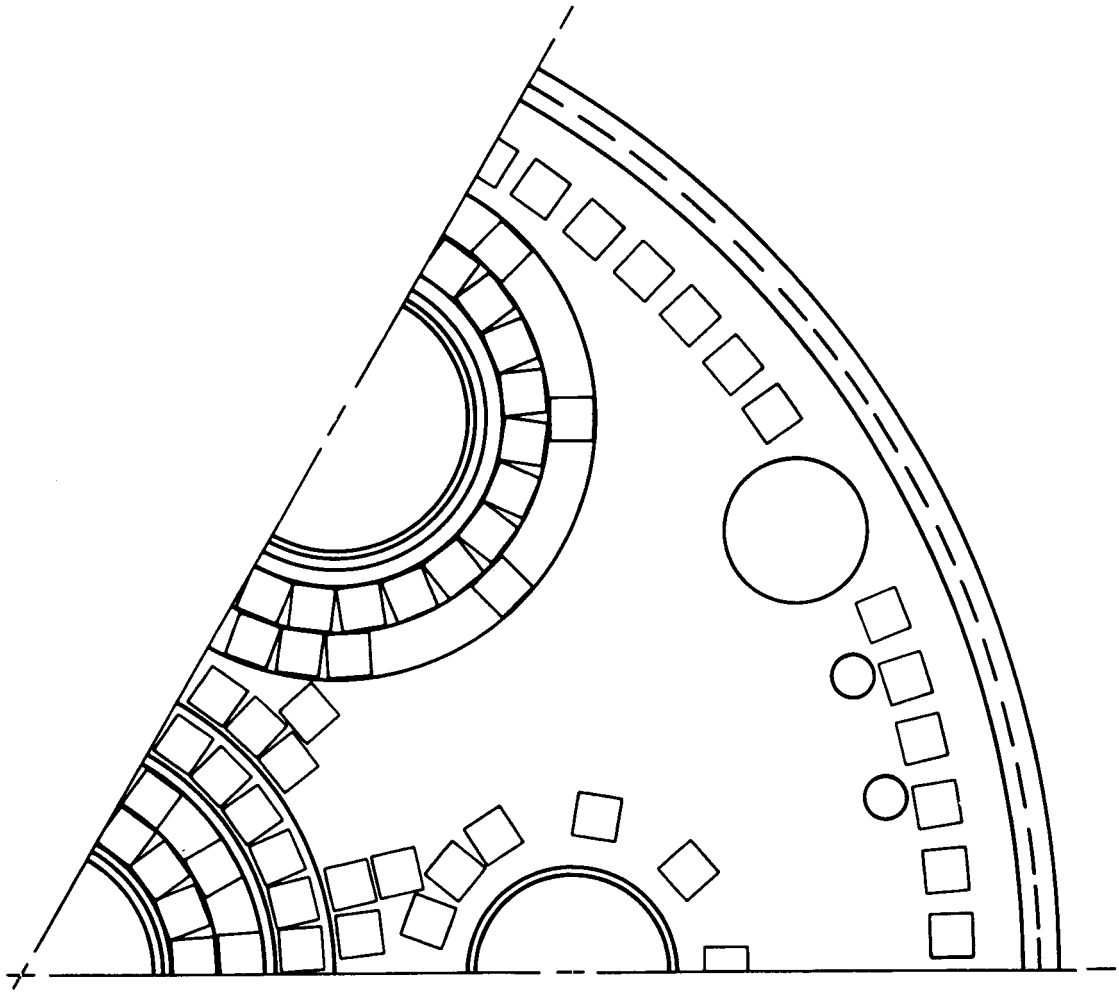

Fig. 6. Linear tendon locations

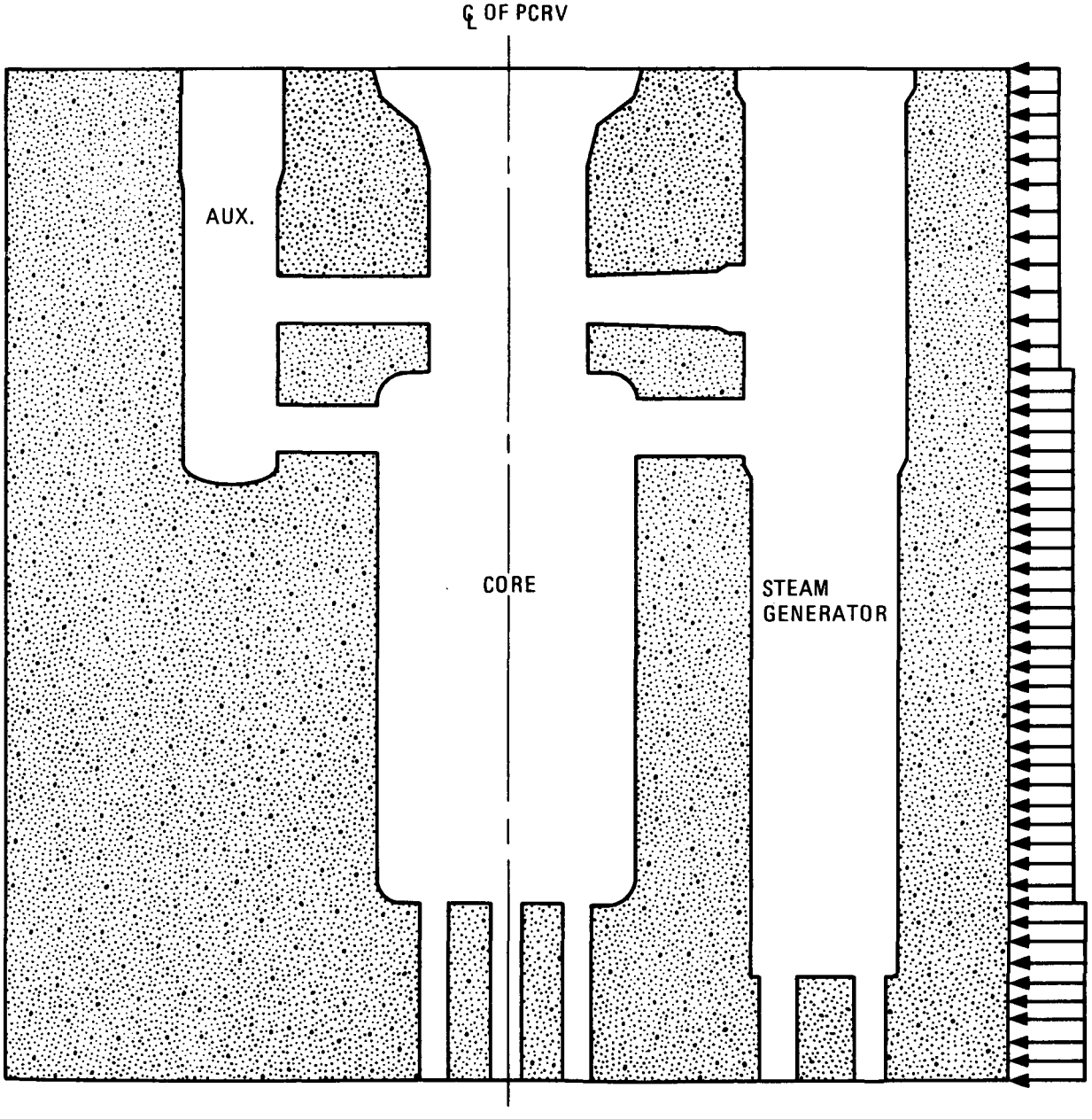

Fig. 7. Circumferential prestress distribution

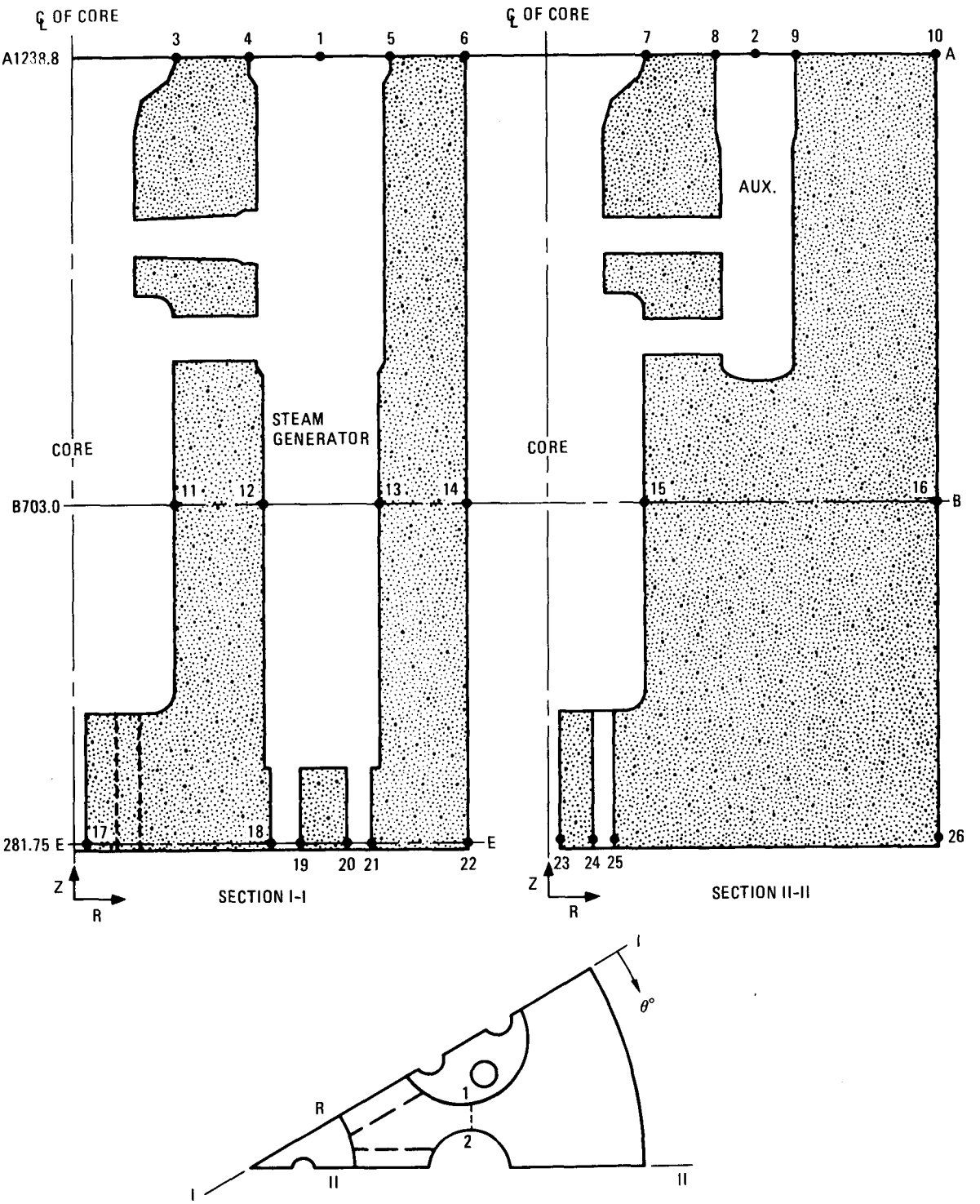

Fig. 8. Key stress locations

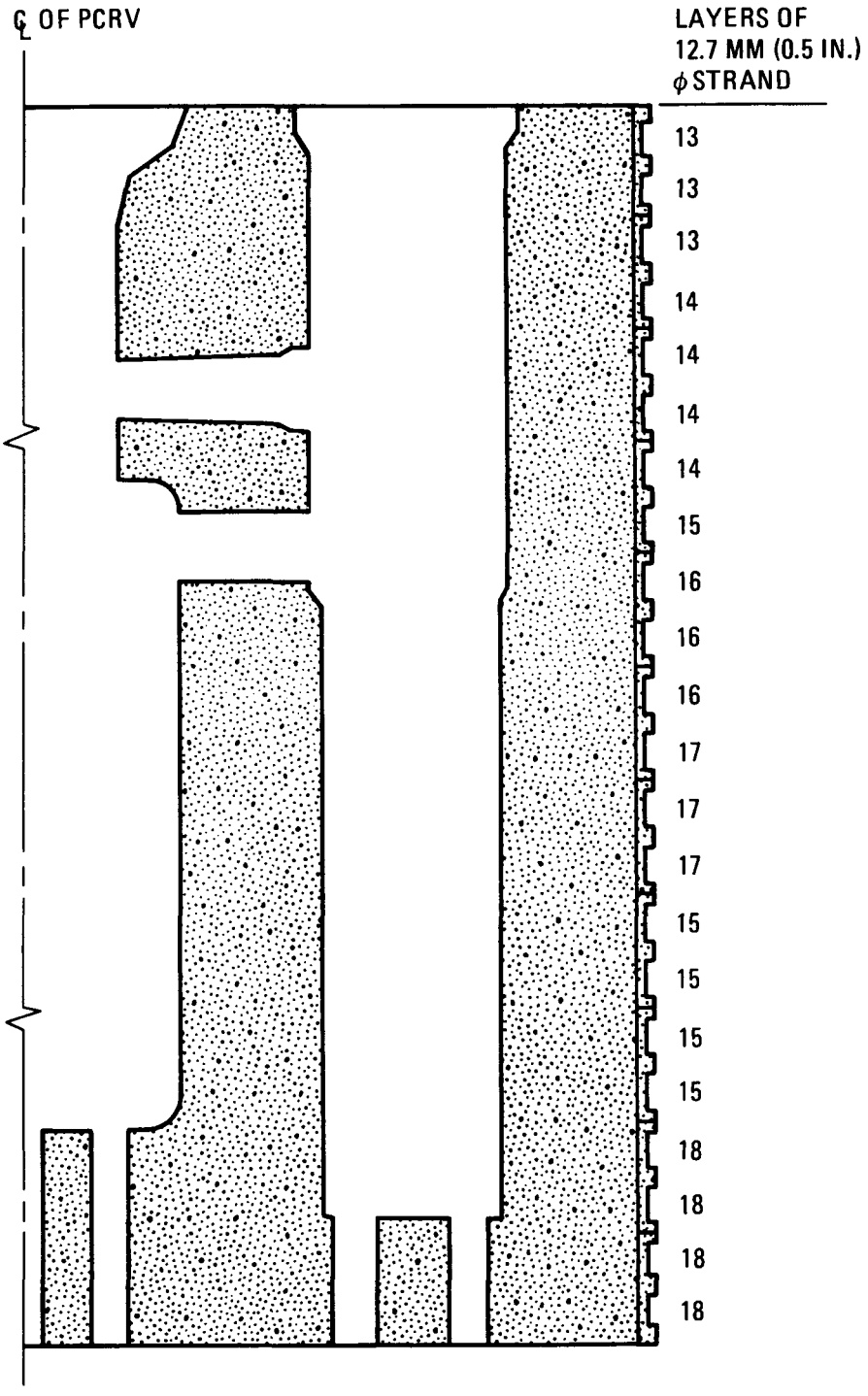

Fig. 9. Circumferential prestress requirements

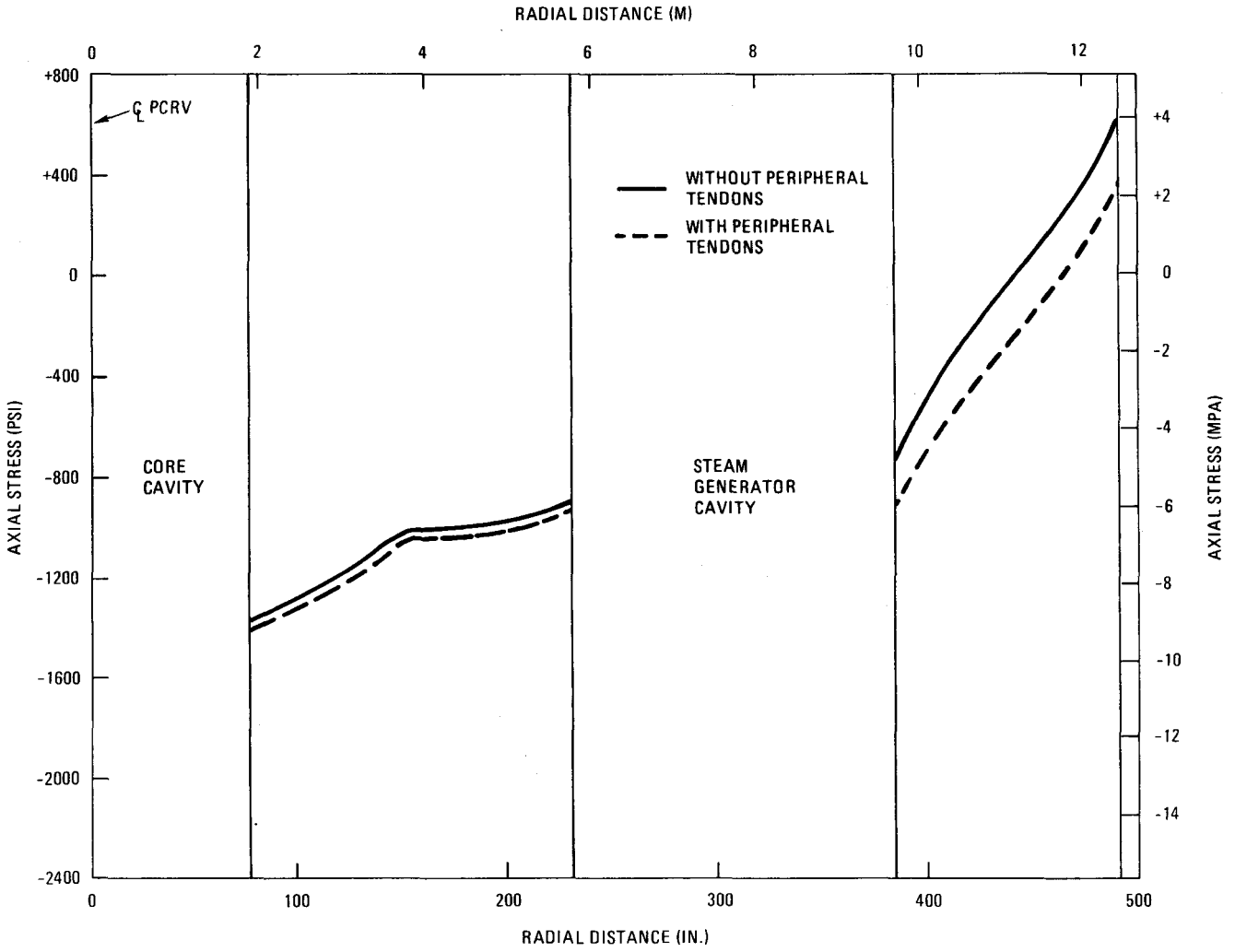

Fig. 10. Axial stress, section I(A), variable R, Z = 990, angle = 0°, loading = F_e + MCP + T_o, with and without peripheral tendons

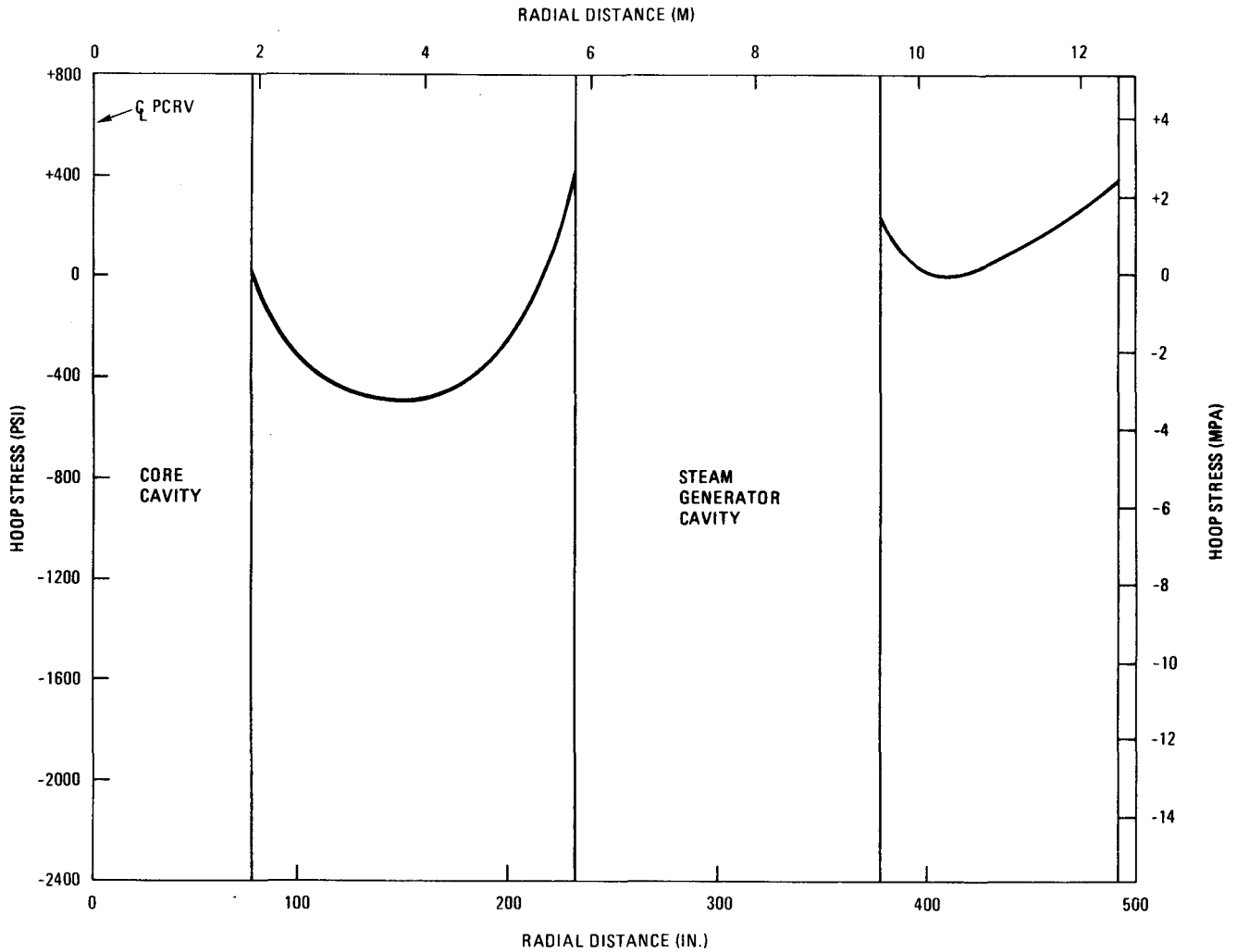

Fig. 11. Hoop stress, section I(A), variable R, Z = 990, angle = 0°, loading = F_e + MCP + T_o, without peripheral tendons

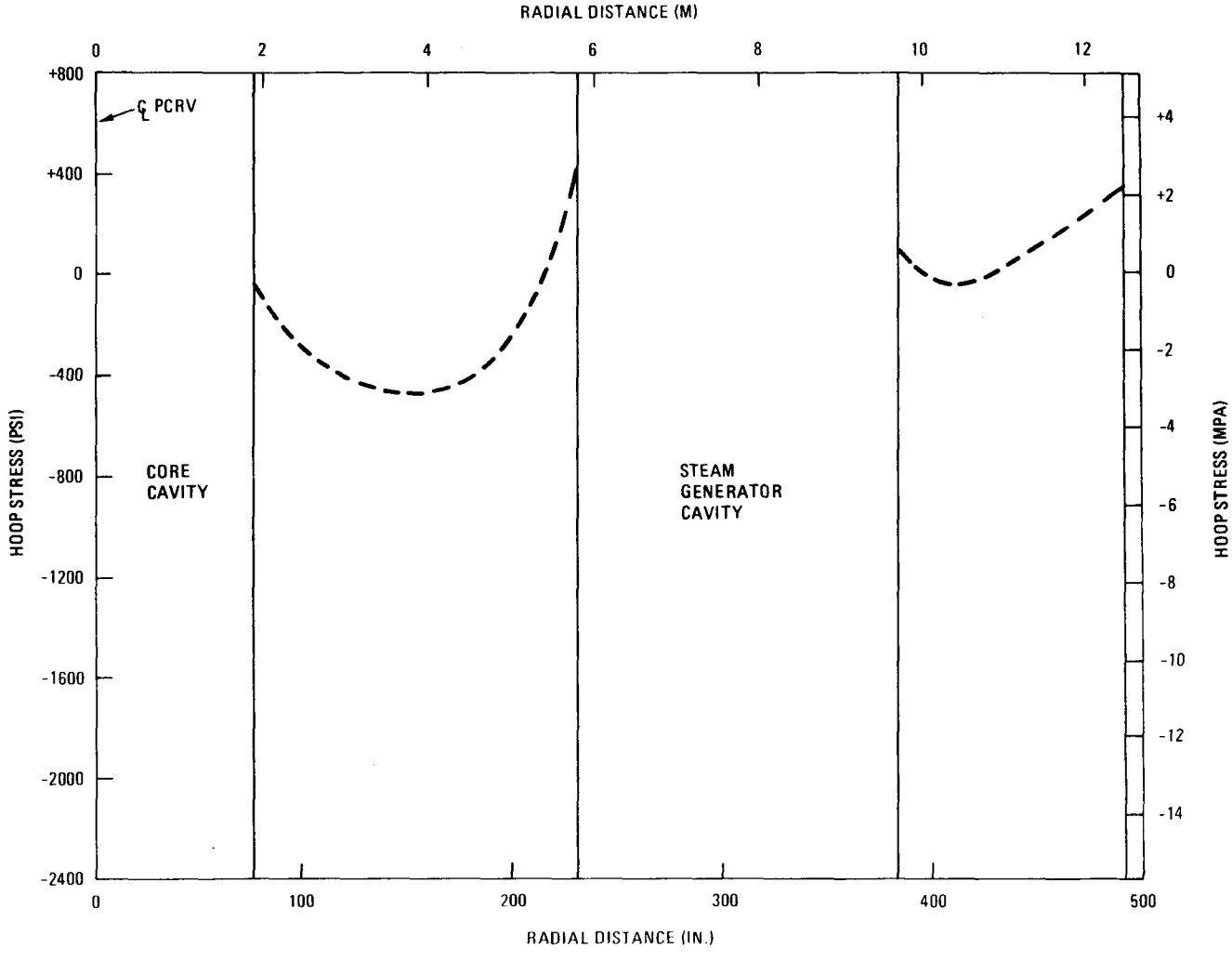

Fig. 12. Hoop stress, section I(A), variable R, Z = 990, angle = 0°, loading = F_e + MCP + T_o, with peripheral tendons

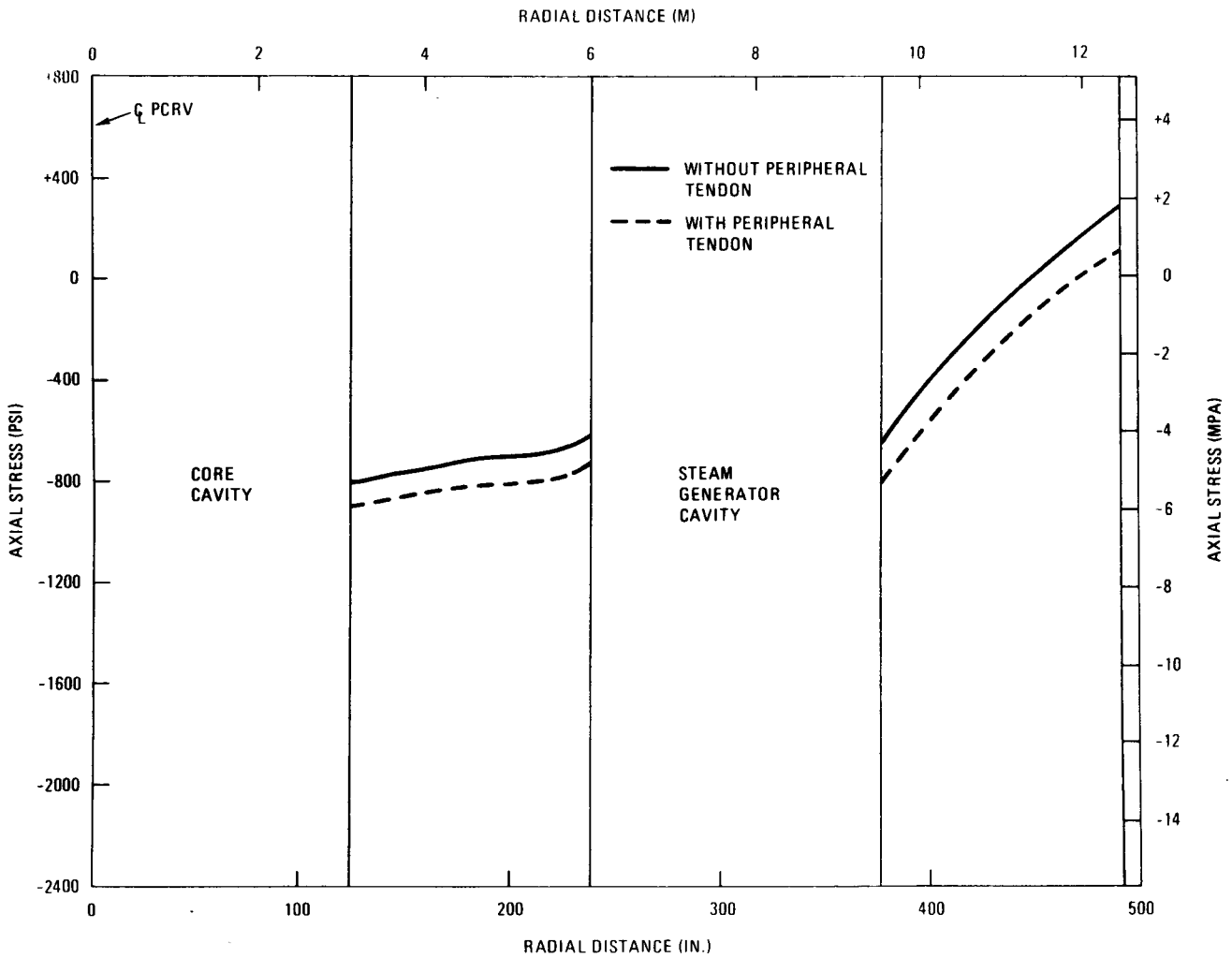

Fig. 13. Axial stress, section I(B), variable R, Z = 703, angle = 0°, loading = F_e + MCP + T_o, with and without peripheral tendons

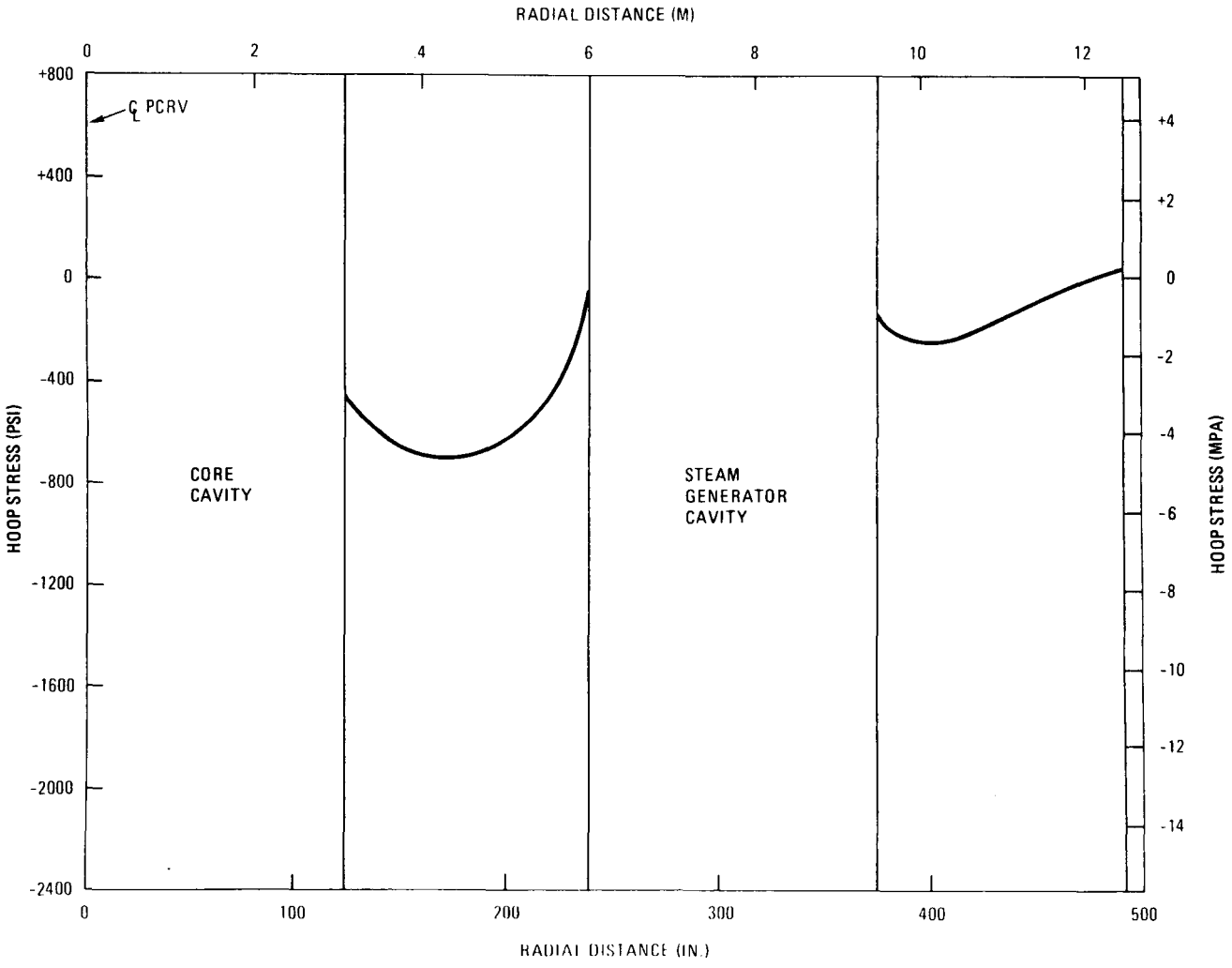

Fig. 14. Hoop stress, section I(B), variable R, Z = 703, angle = 0°, loading = F_e + MCP + T_o, without peripheral tendons

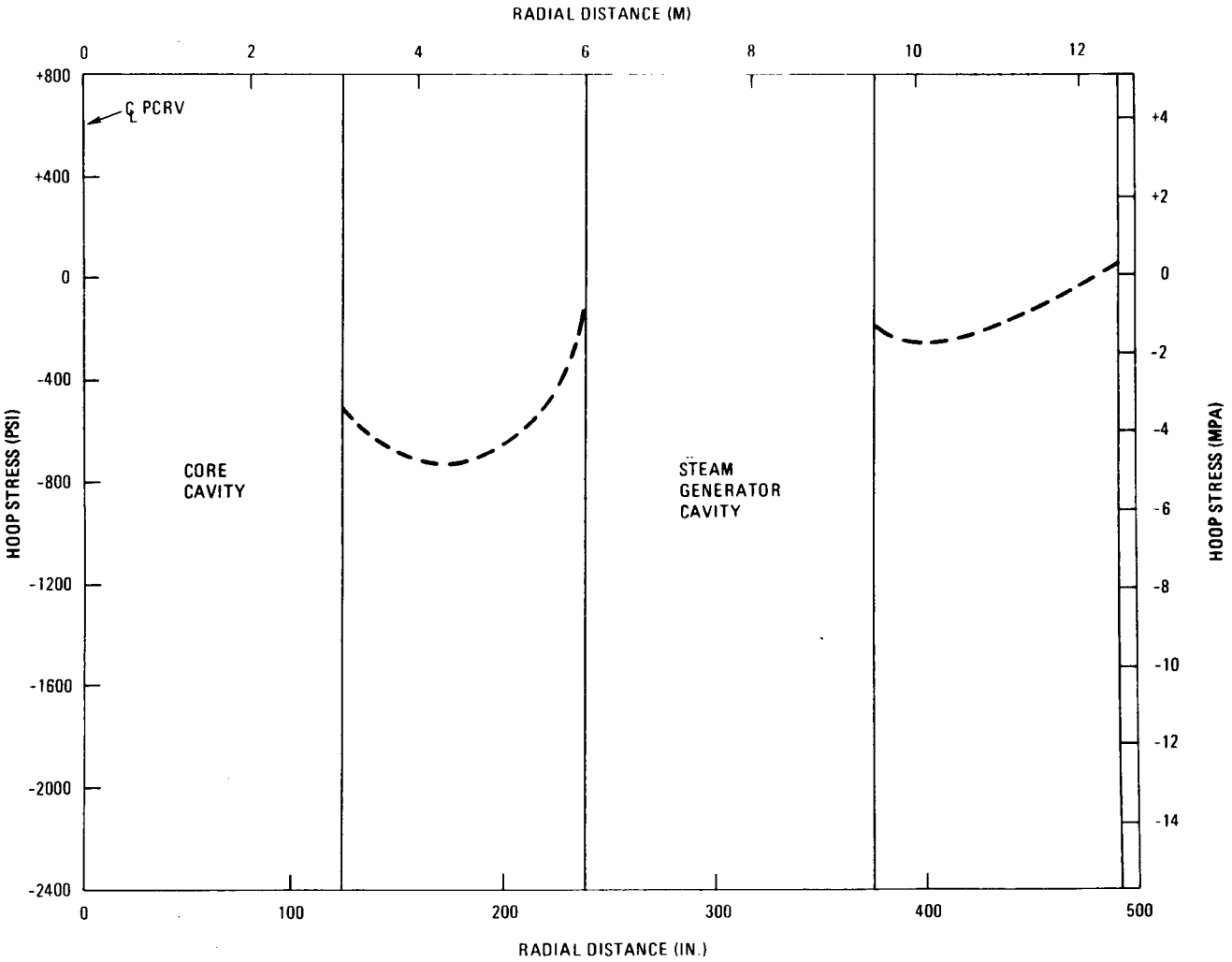

Fig. 15. Hoop stress, section I(B), variable R, Z = 703, angle = 0°, loading = F_e + MCP + T_o, with peripheral tendons

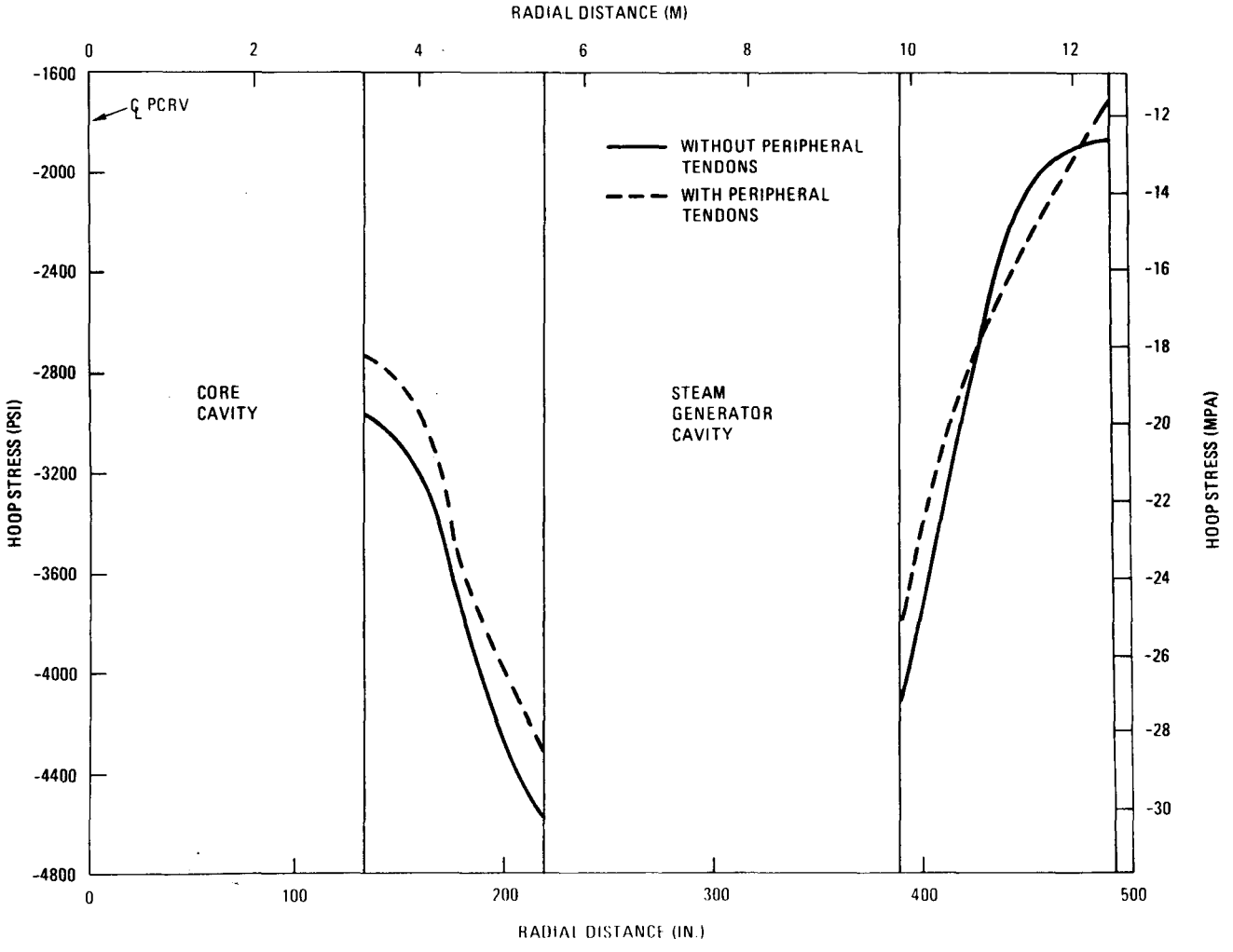

Fig. 16. Hoop stress, section I(A), variable R, Z = 1238.8, angle = 0°, loading = F_i, with and without peripheral tendons

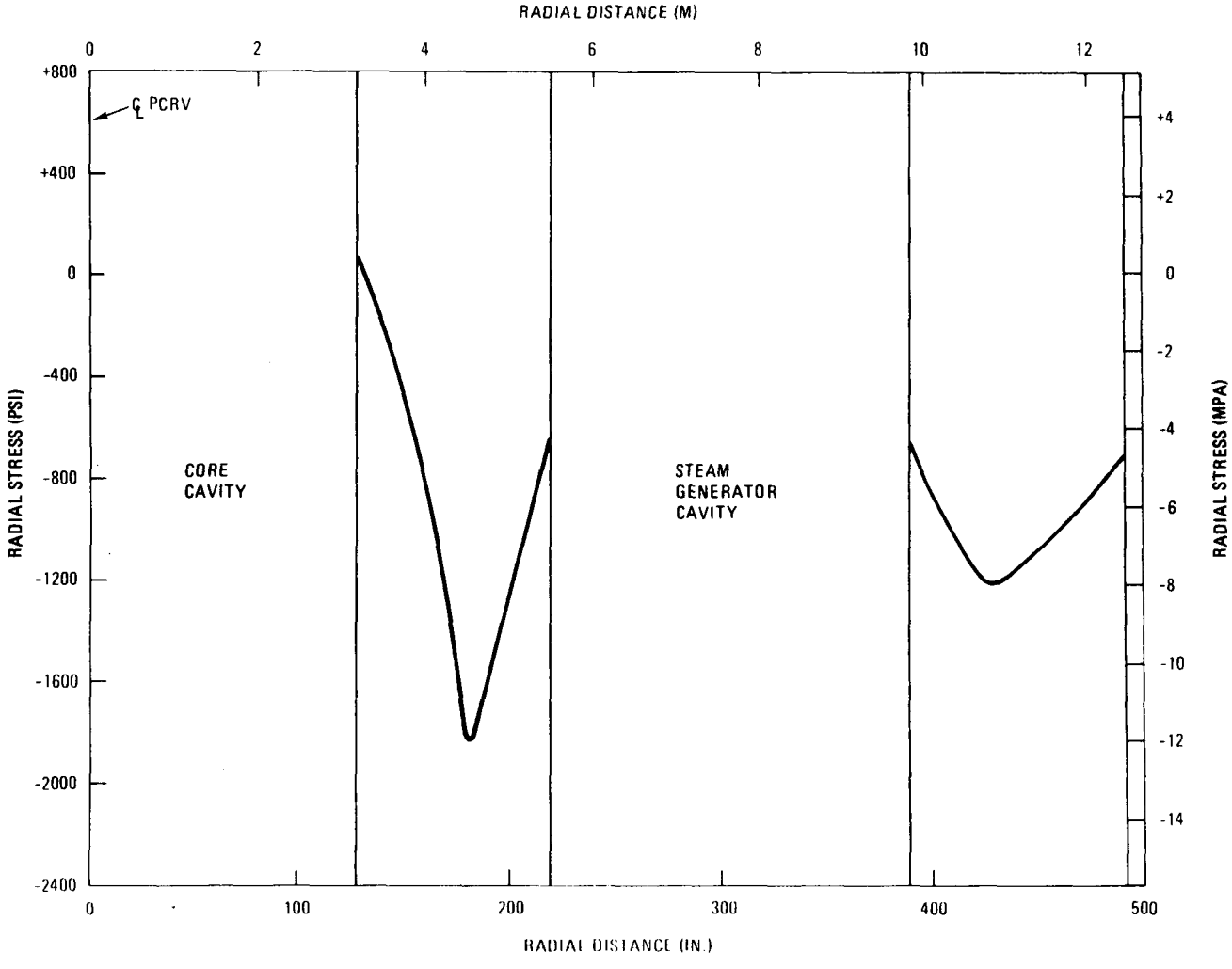

Fig. 17. Radial stress, section I(A), variable R, Z = 1238.8, angle = 0°, loading = F_i

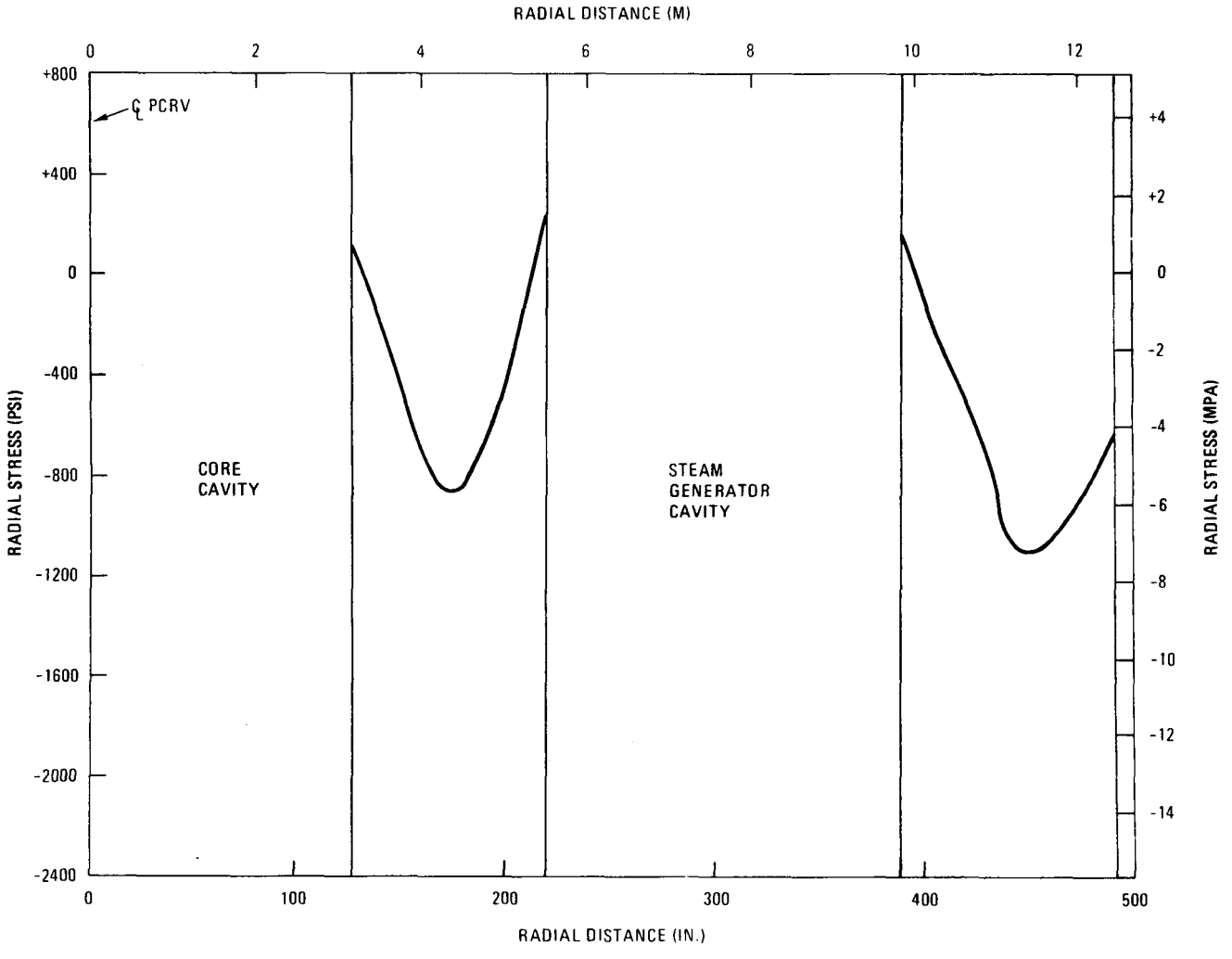

Fig. 18. Radial stress, section I(A), variable R, Z = 1238.8, angle = 0°, loading = F_e + MCP + T_o

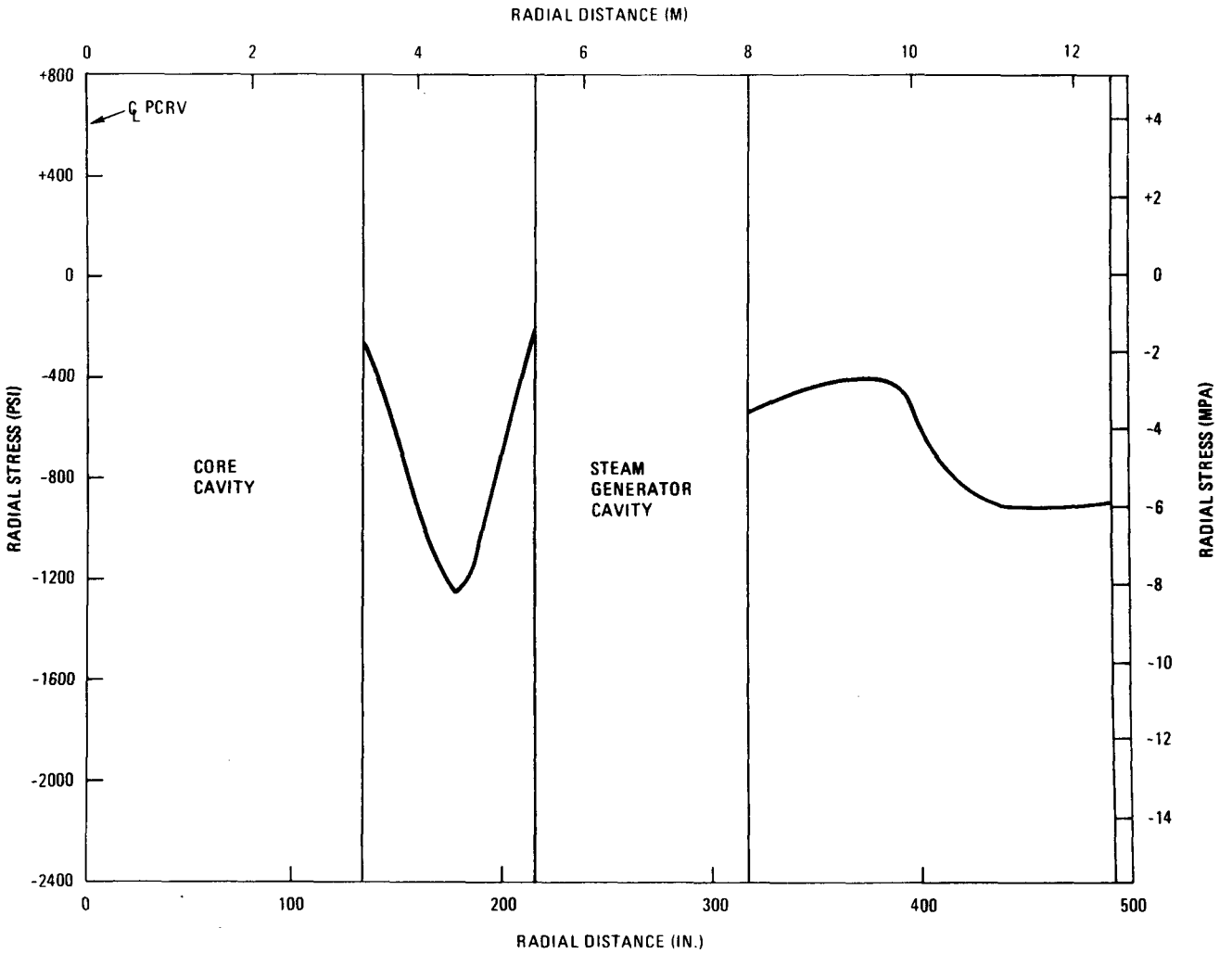

Fig. 19. Radial stress, section II(A), variable R, Z = 1238.8, angle = -60°, loading = F_i

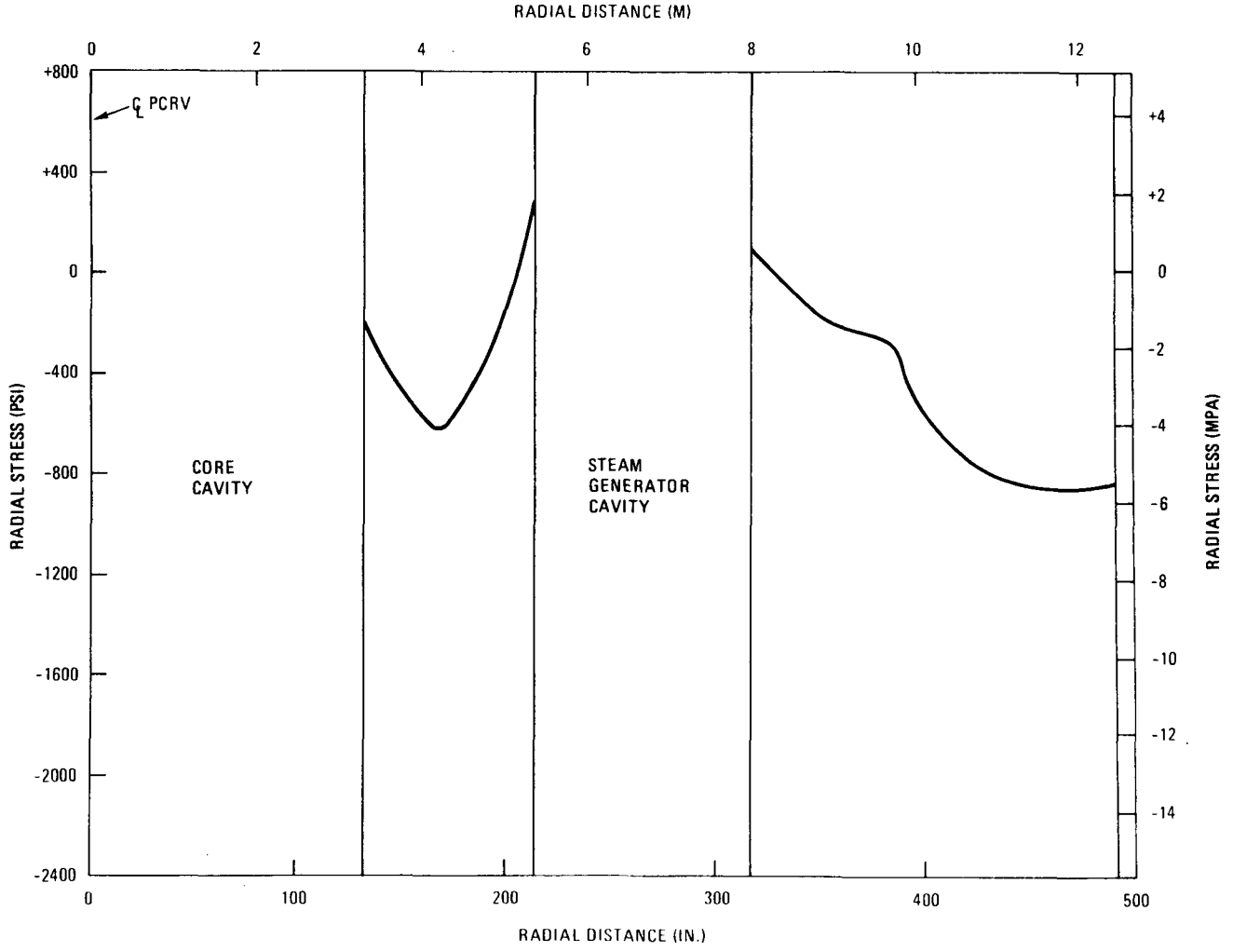

Fig. 20. Radial stress, section II(A), variable R, Z = 1238.8, angle = -60°, loading = F_e + MCP + T_o

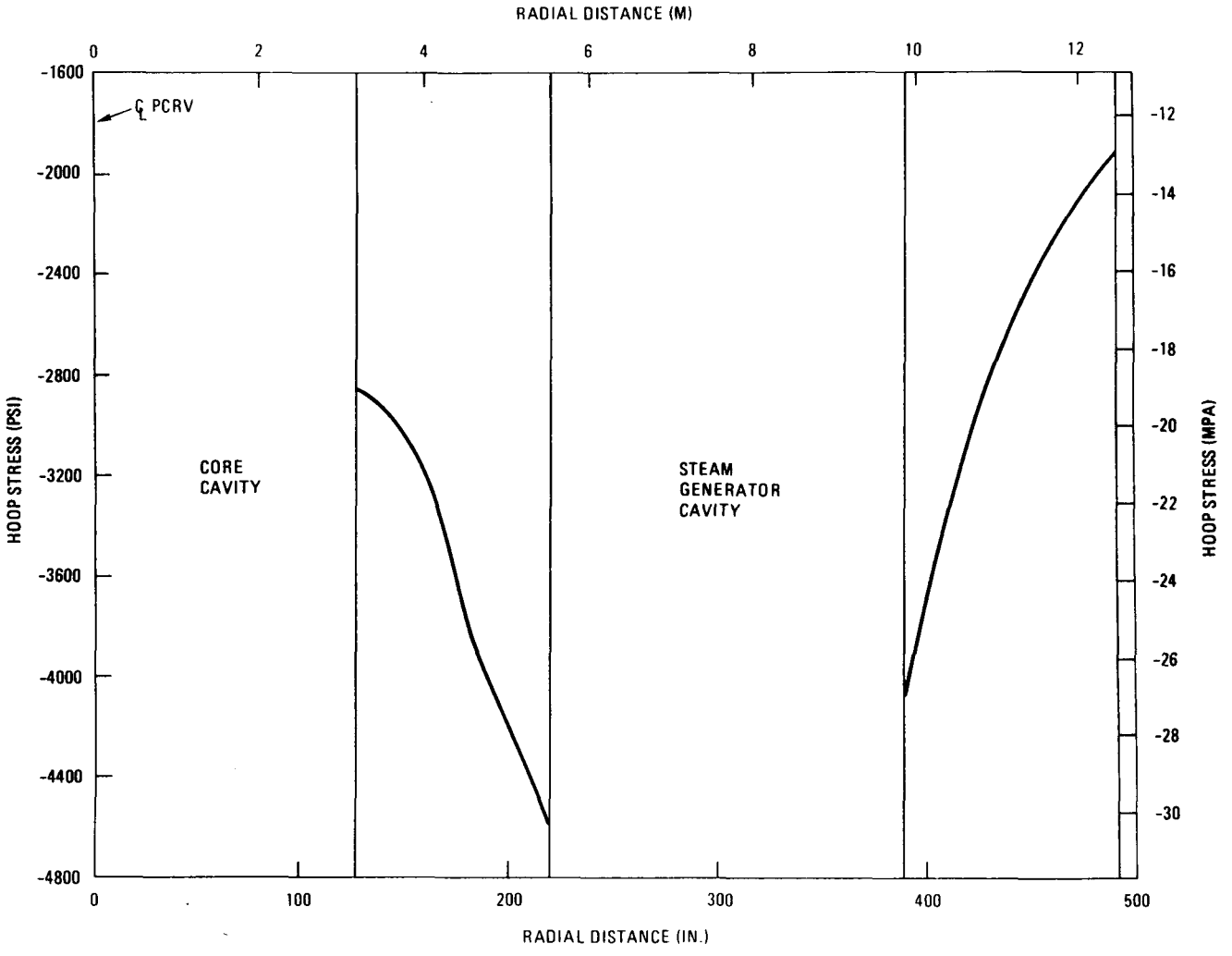

Fig. 21. Hoop stress, section I(A), variable R, Z = 1238.8, angle = 0°, loading = F_i

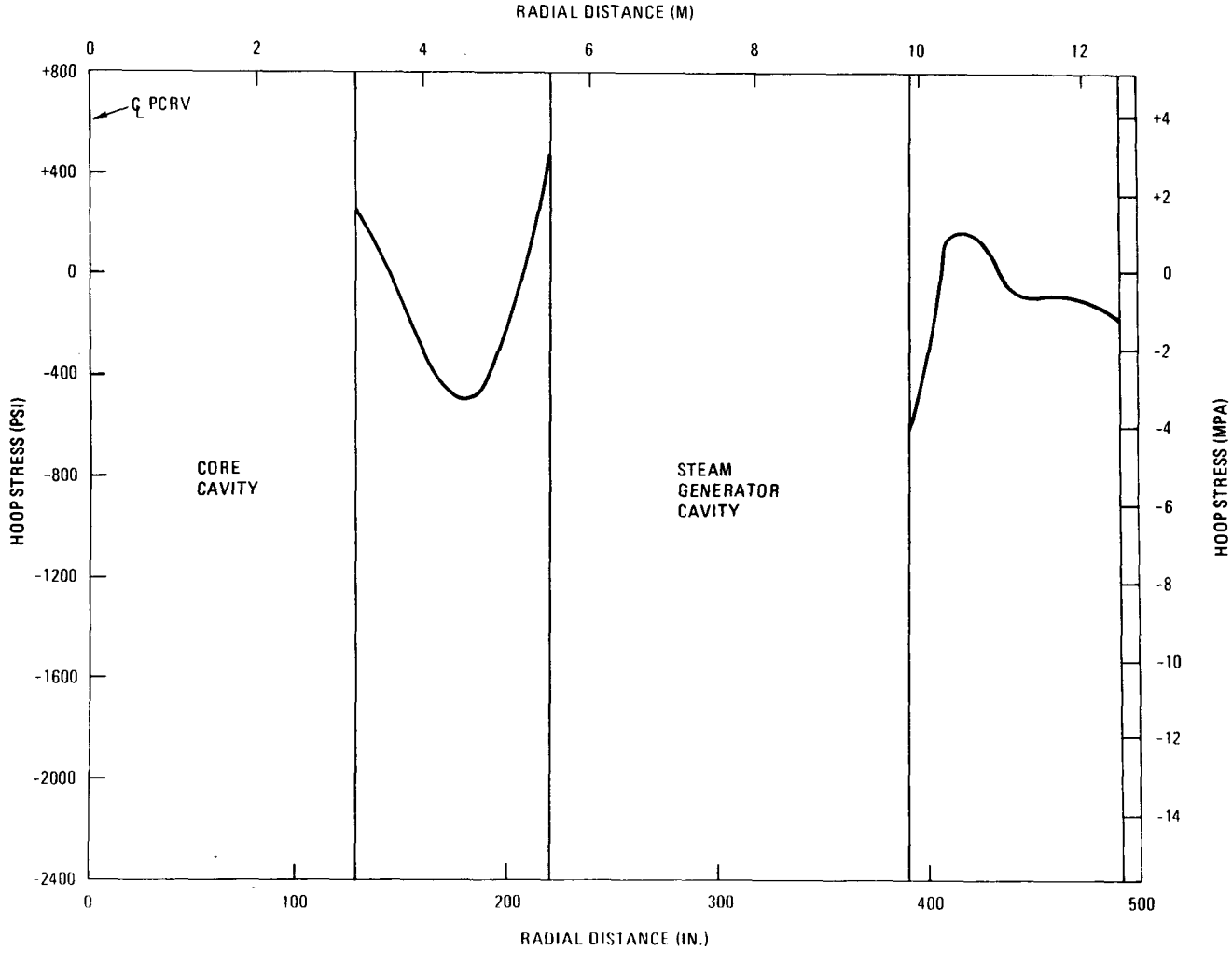

Fig. 22. Hoop stress, section I(A), variable R, Z = 1238.8, angle = 0°, loading = F_e + MCP + T_o

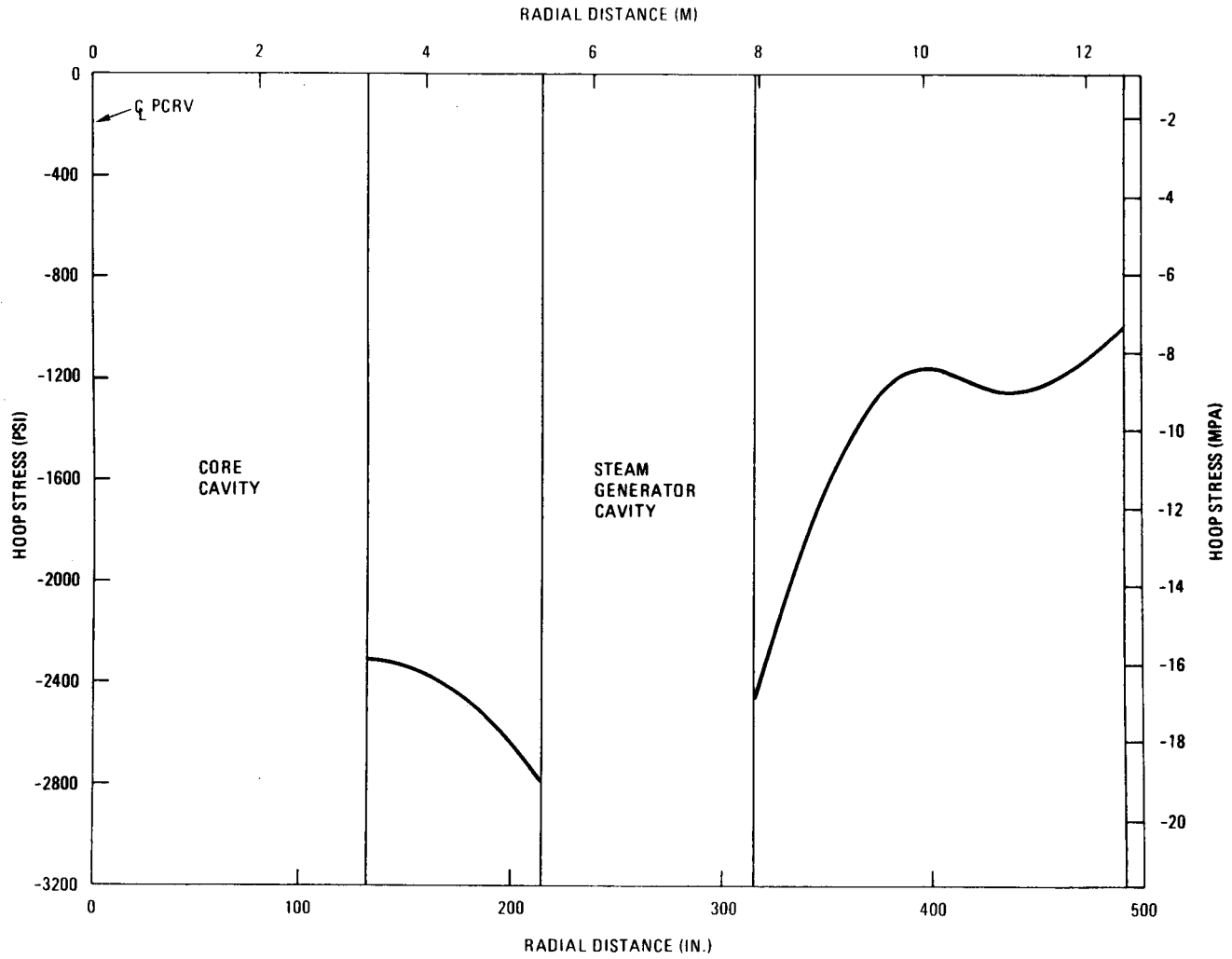

Fig. 23. Hoop stress, section II(A), variable R, Z = 1238.8, angle = -60°, loading = F_i

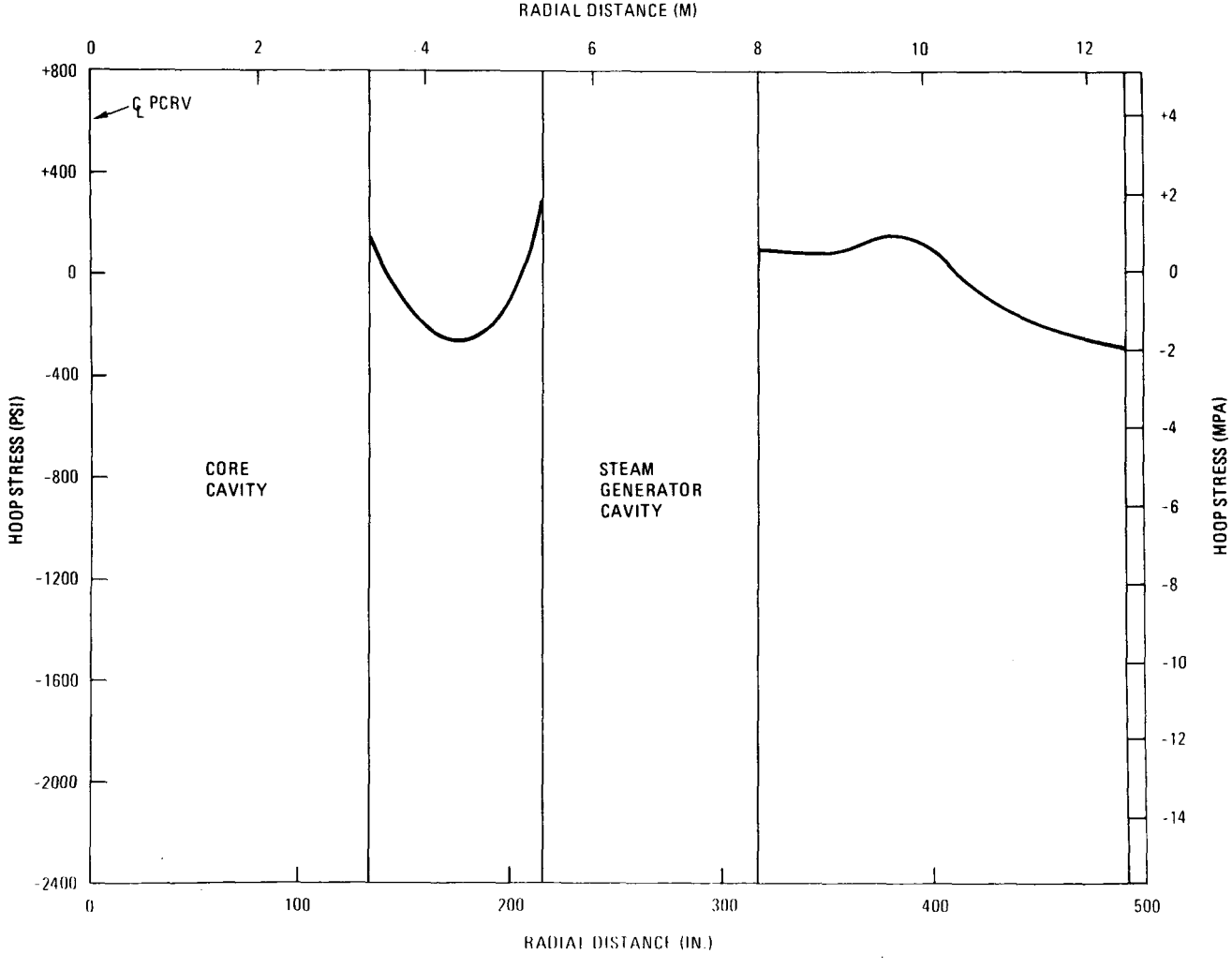

Fig. 24. Hoop stress, section II(A), variable R, Z = 1238.8, angle = -60°, loading = F_e + MCP + T_o

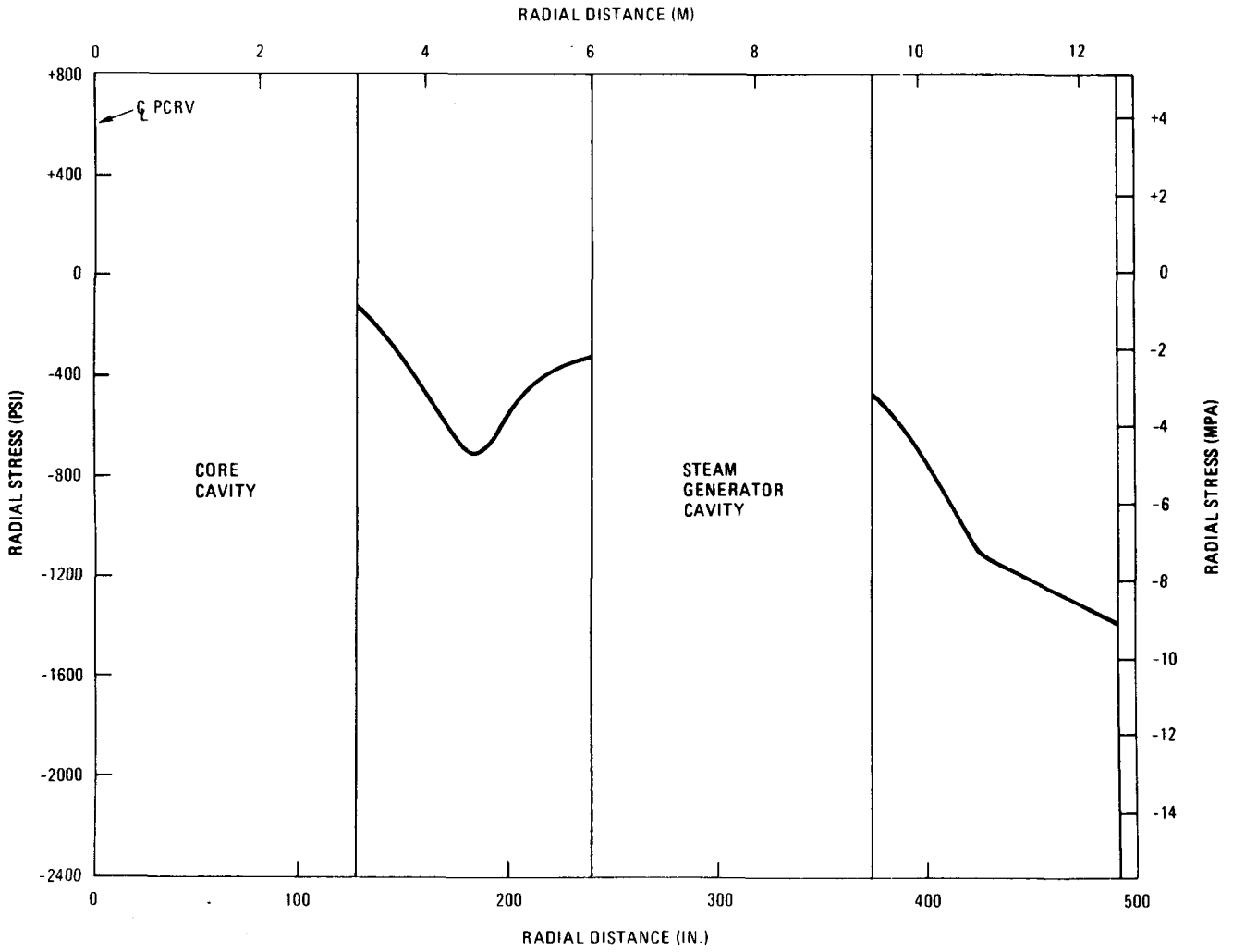

Fig. 25. Radial stress, section I(B), variable R, Z = 703, angle = 0°, loading = F_i

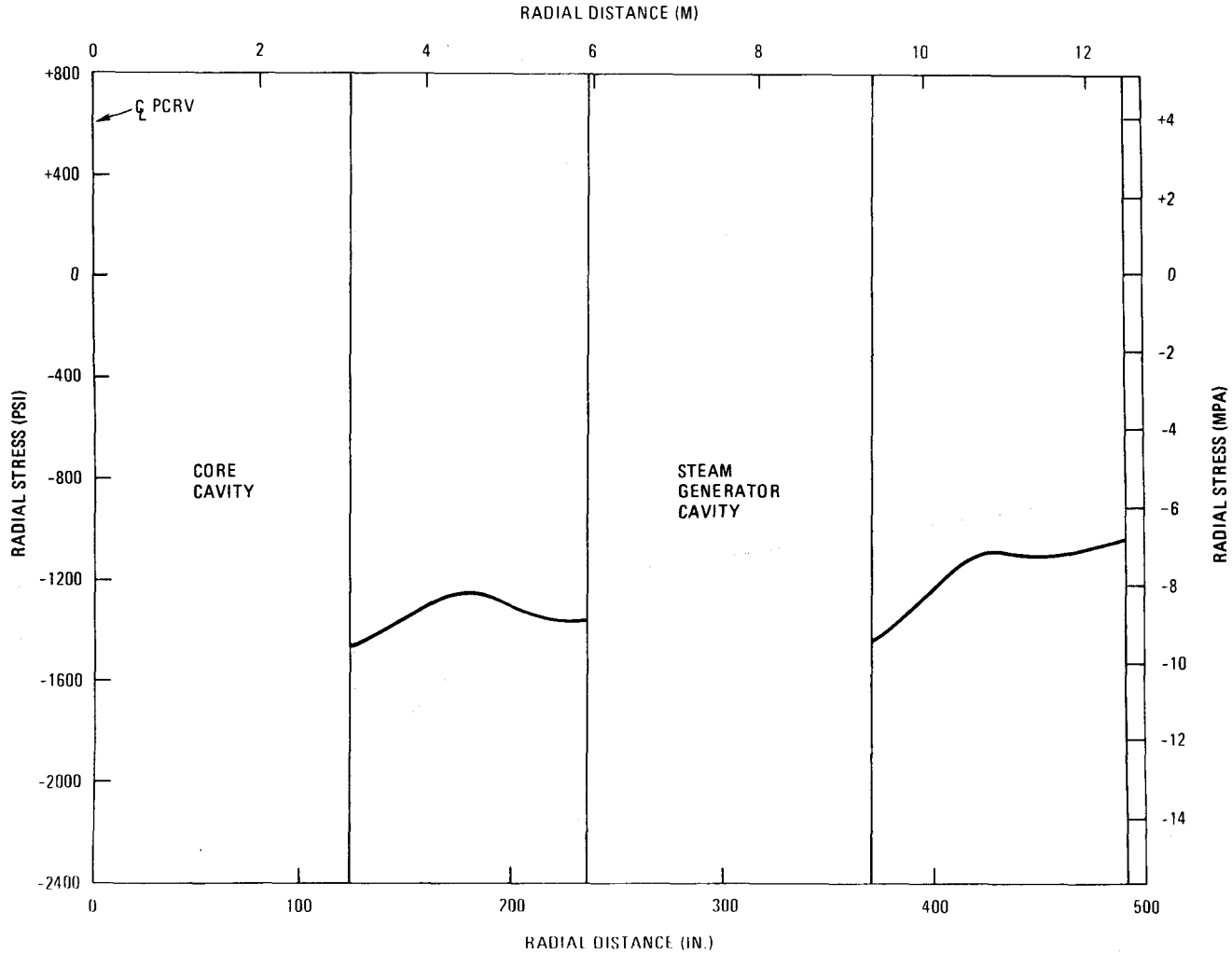

Fig. 26. Radial stress, section I(B), variable R, Z = 703, angle = 0°, loading = F_e + MCP + T_o

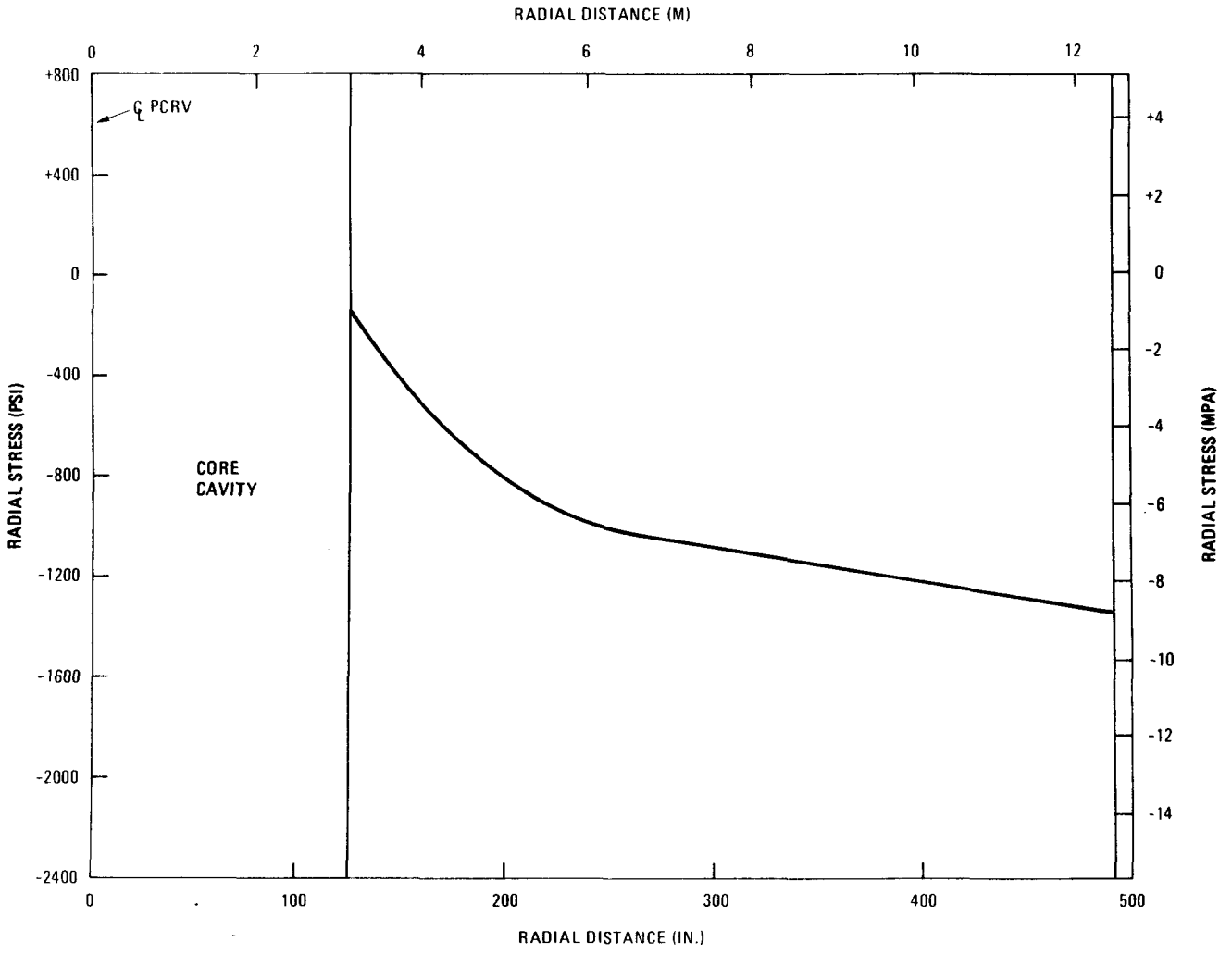

Fig. 27. Radial stress, section II(B), variable R, Z = 703, angle = -60°, loading = F_i

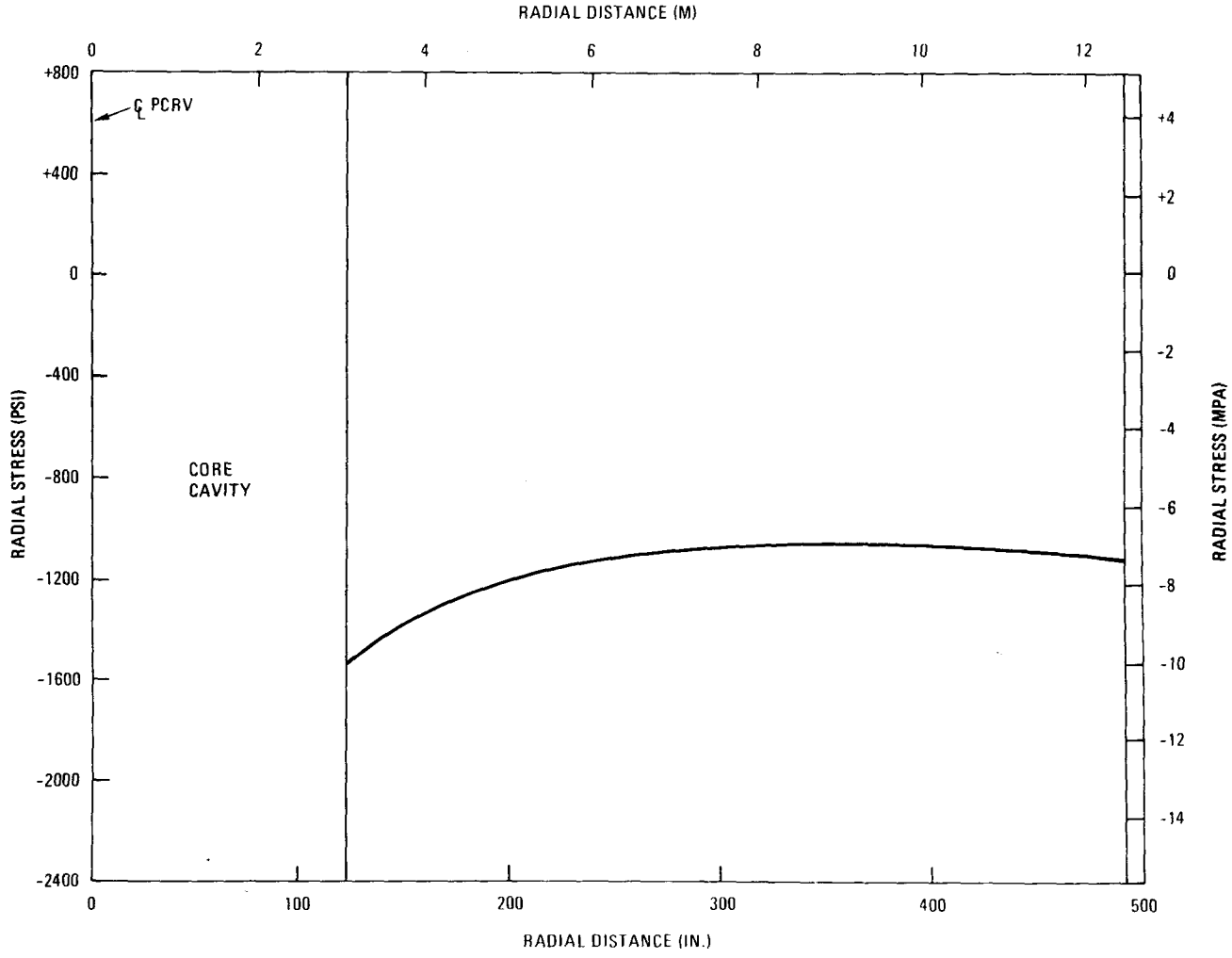

Fig. 28. Radial stress, section II(B), variable R, Z = 703, angle = -60°, loading = F_e + MCP + T_o

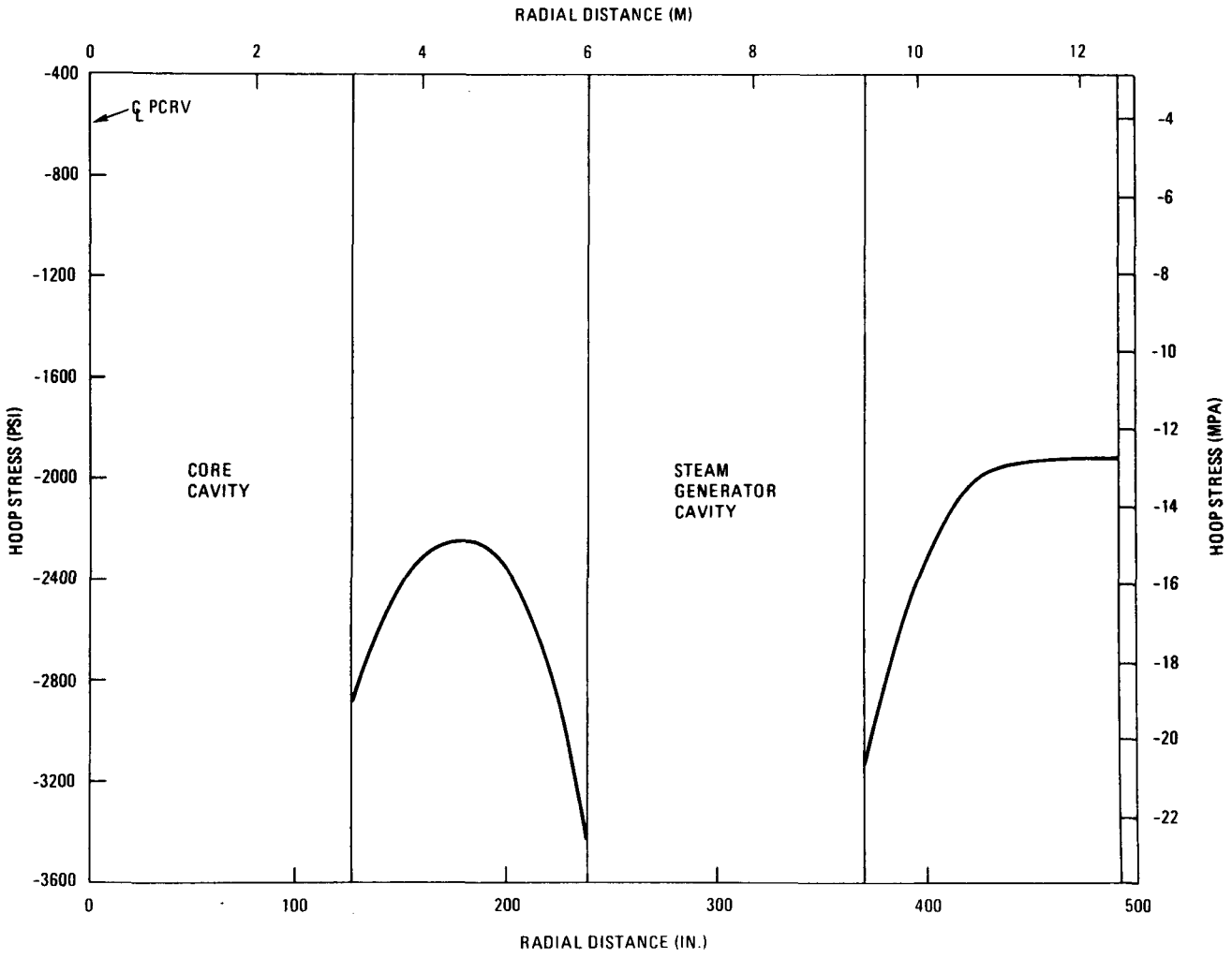

Fig. 29. Hoop stress, section I(B), variable R, Z = 703, angle = 0°, loading = F_i

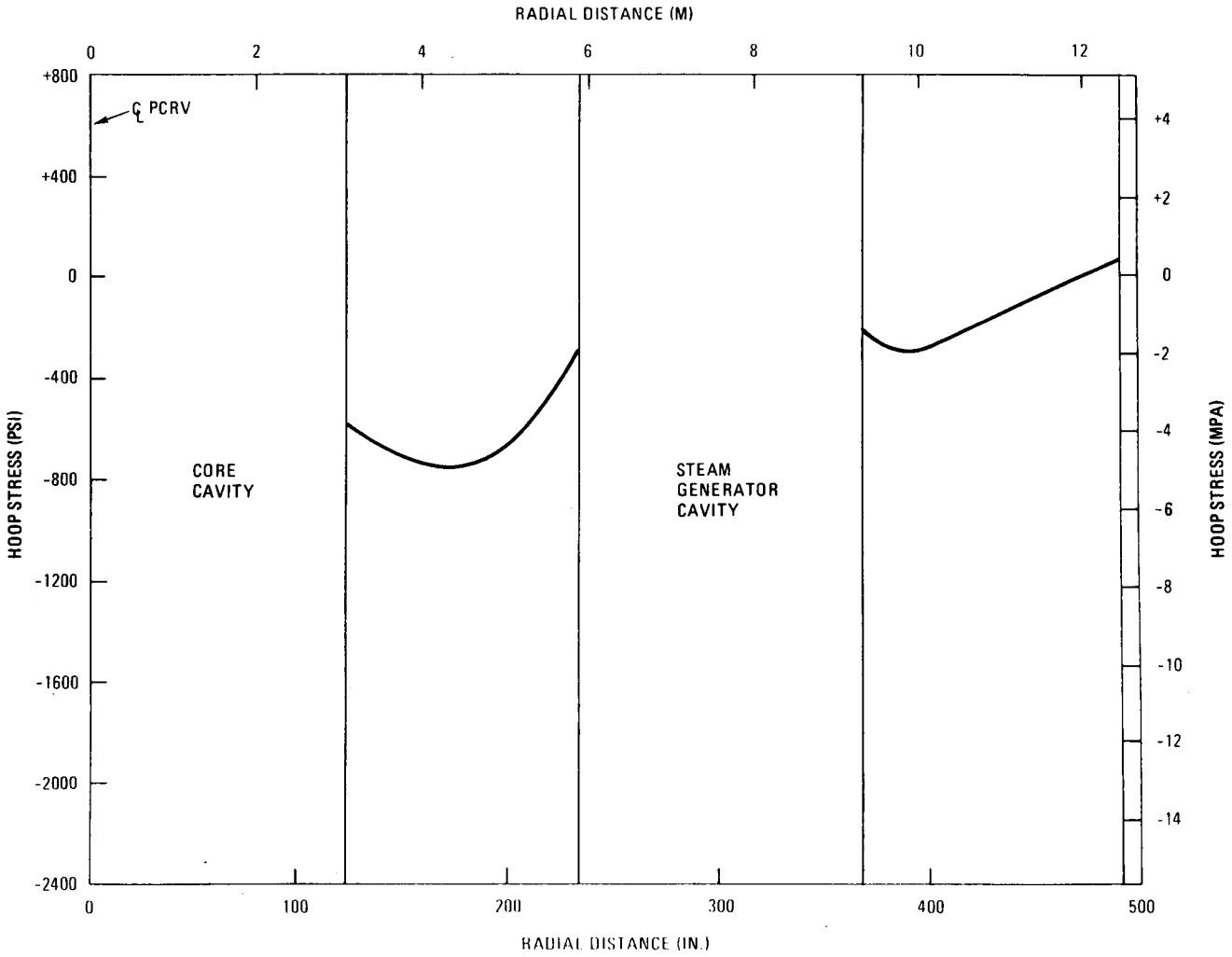

Fig. 30. Hoop stress, section I(B), variable R, Z = 703, angle = 0°, loading = F_e + MCP + T_o

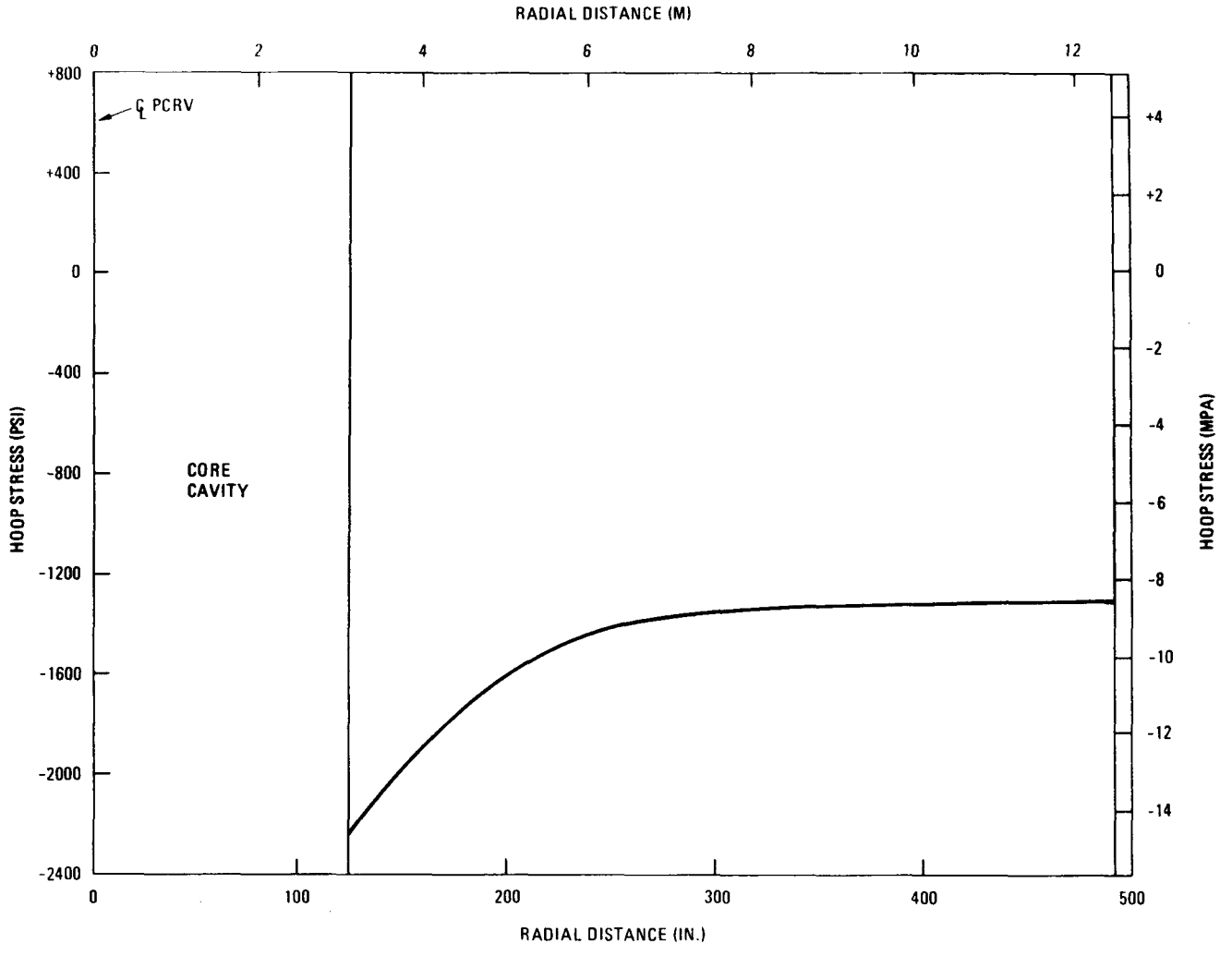

Fig. 31. Hoop stress, section II(B), variable R, Z = 703, angle = -60°, loading = F_i

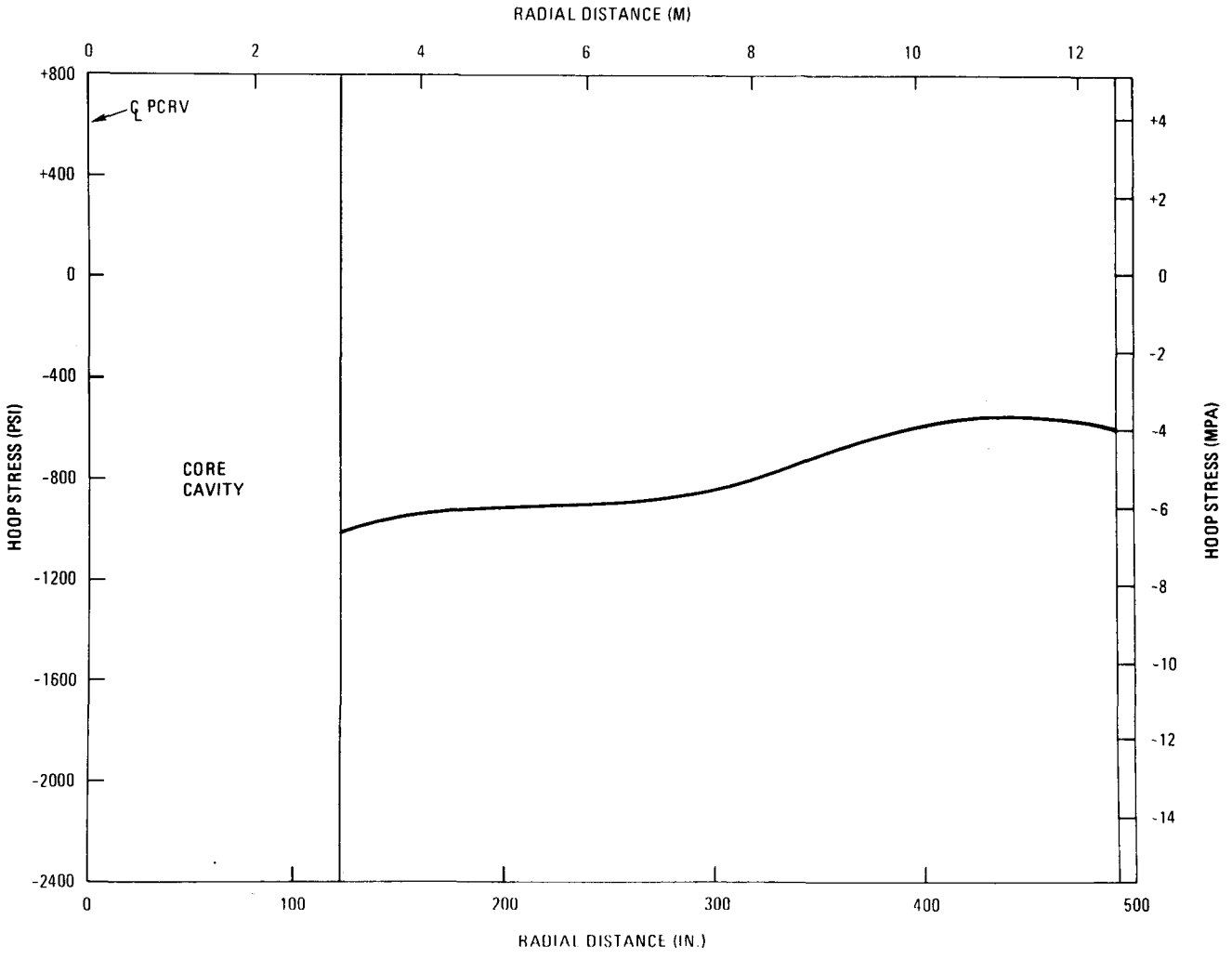

Fig. 32. Hoop stress, section II(B), variable R, Z = 703, angle = -60°, loading = F_e + MCP + T_o

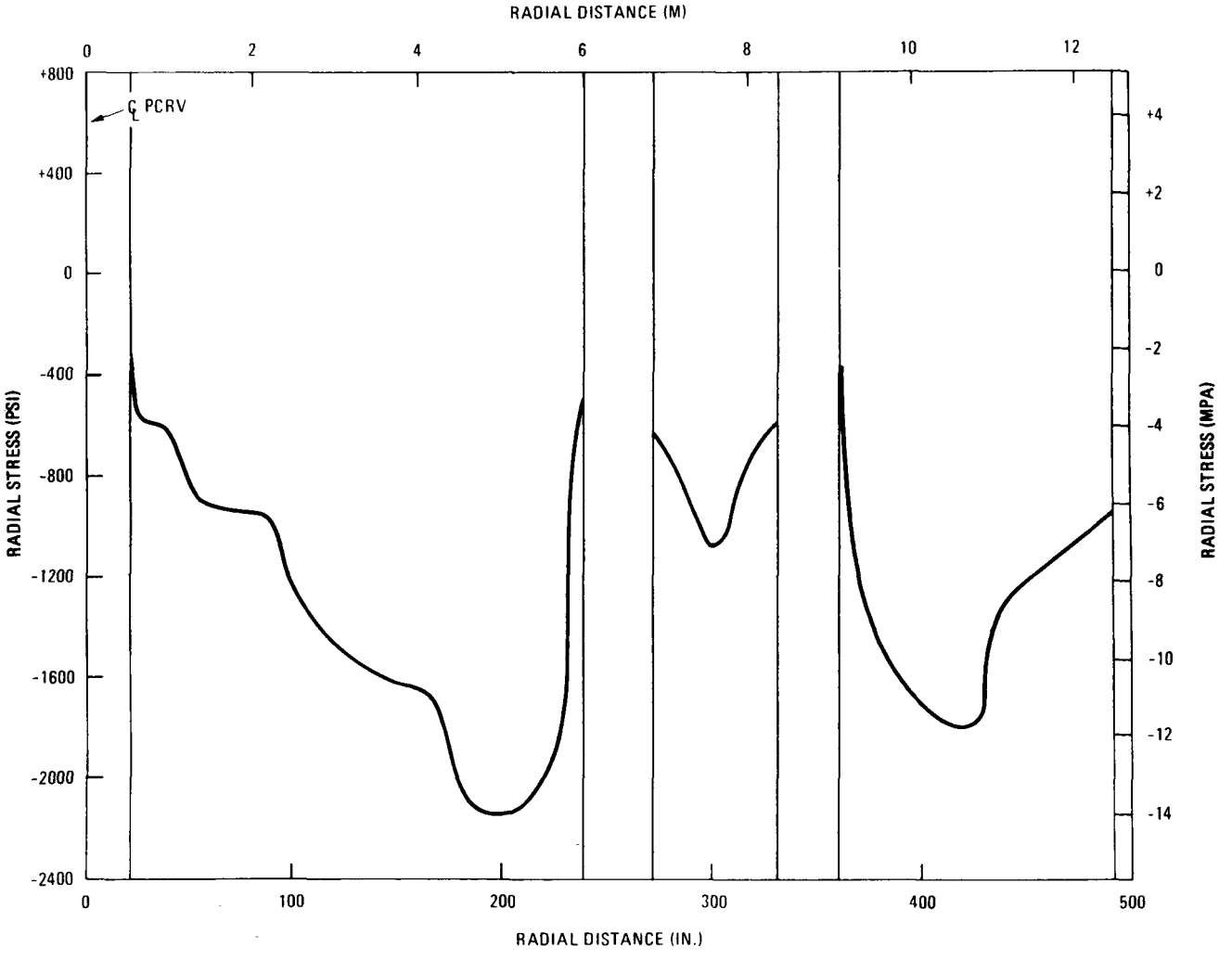

Fig. 33. Radial stress, section I(E), variable R, Z = 281.75, angle = 0°, loading = F_i

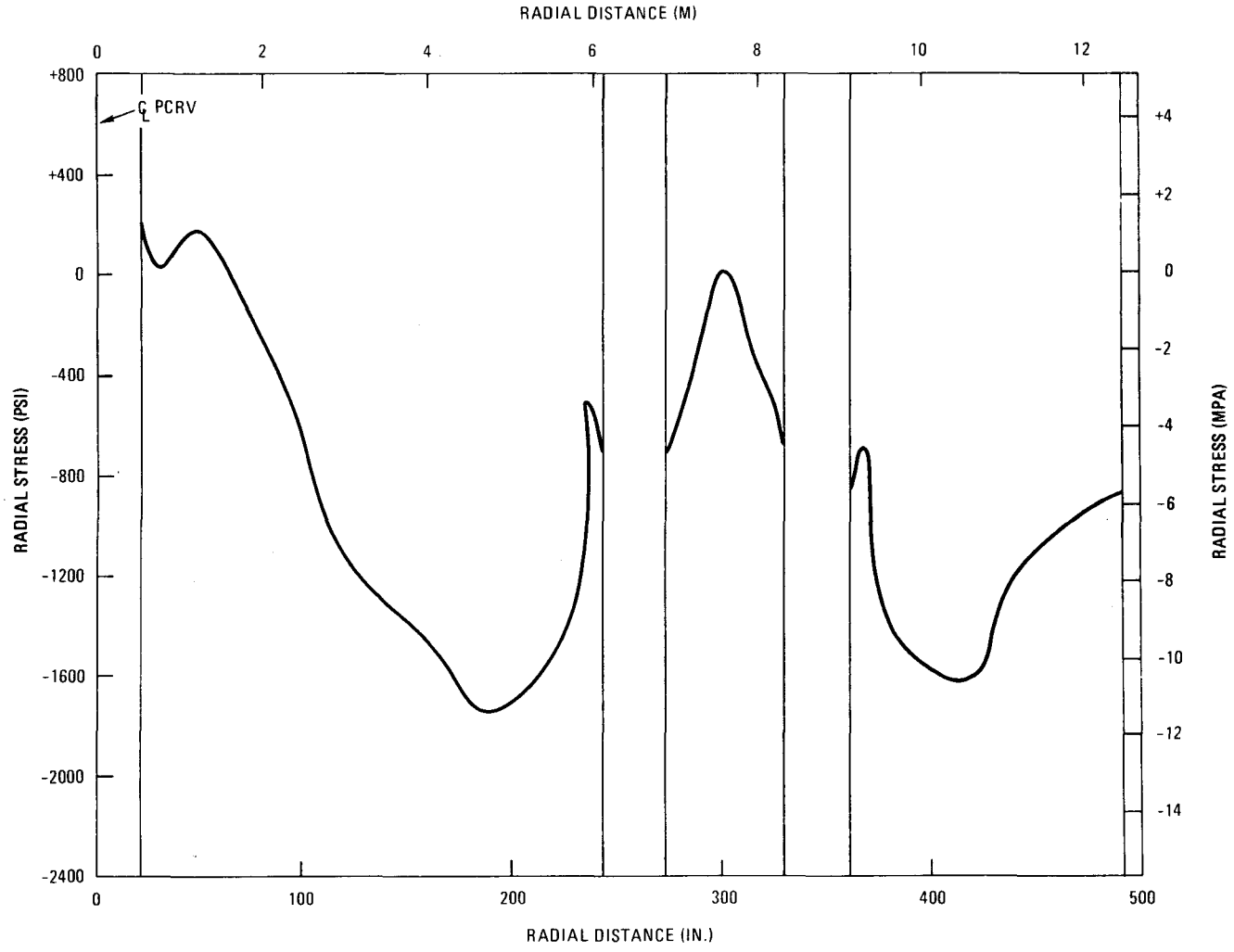

Fig. 34. Radial stress, section I(E), variable R, Z = 281.75, angle = 0°, loading = F_e + MCP + T_o

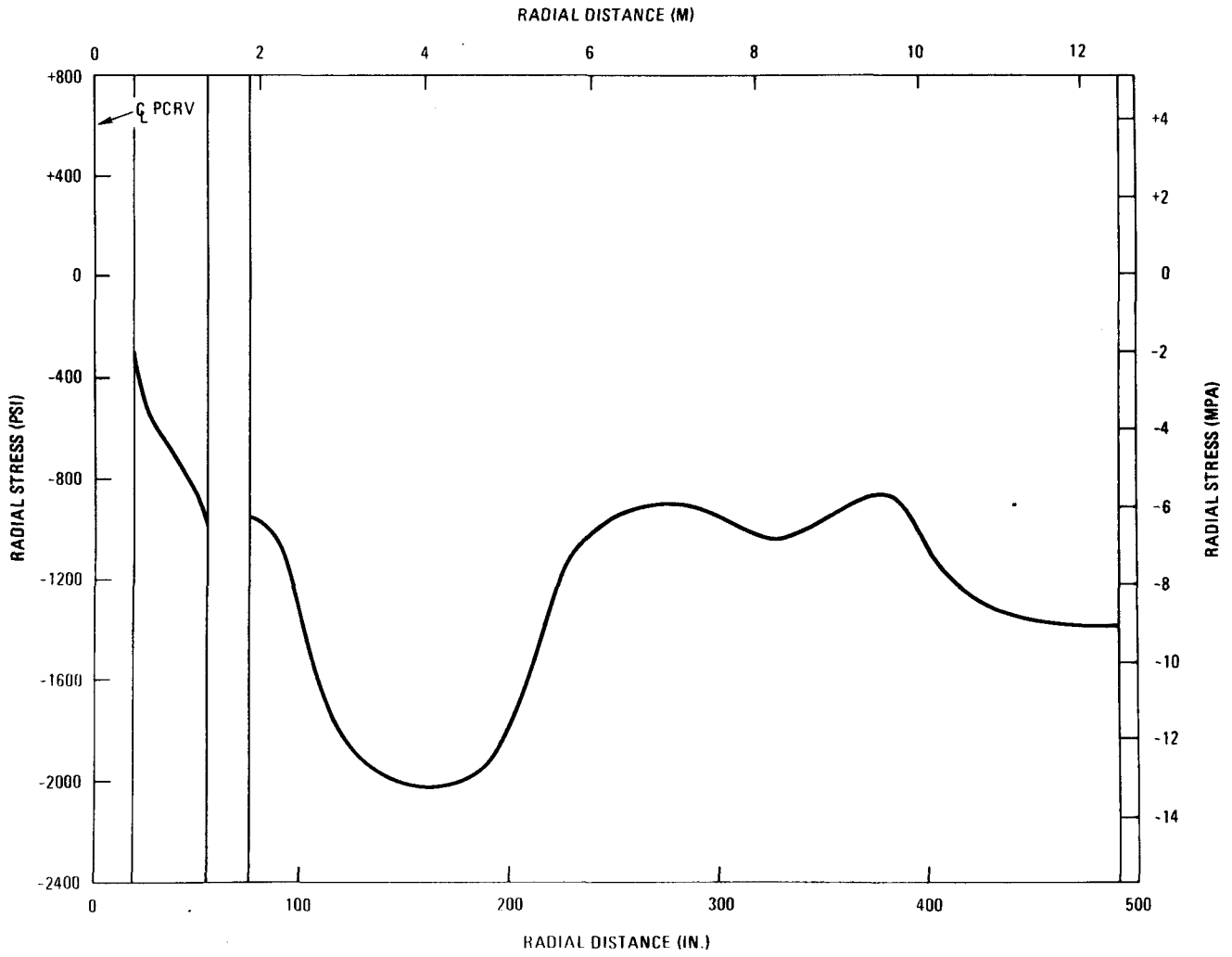

Fig. 35. Radial stress, section II(E), variable R, Z = 281.75, angle = -60°, loading = F_i

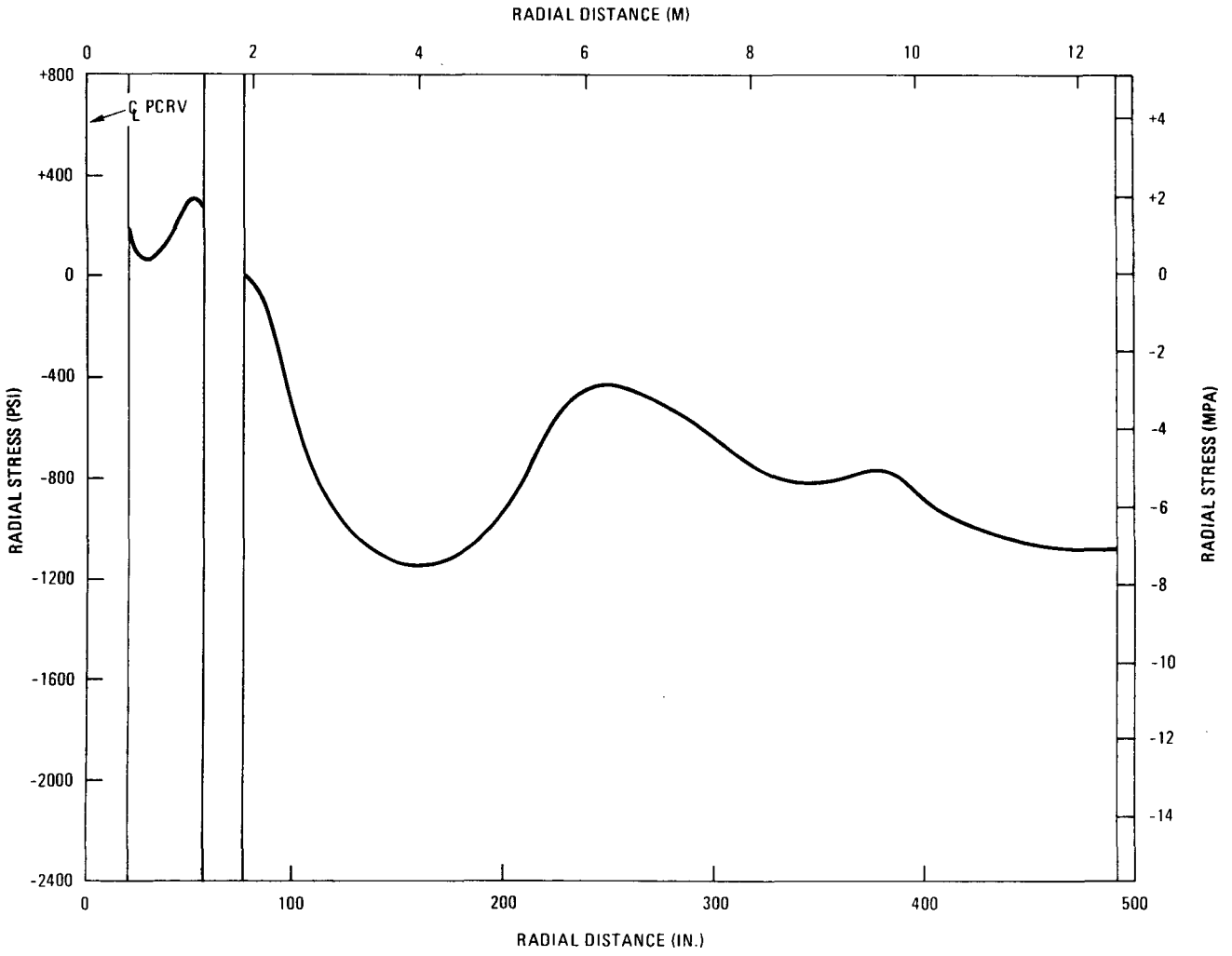

Fig. 36. Radial stress, section II(E), variable R, Z = 281.75, angle = -60°, loading = F_e + MCP + T_o

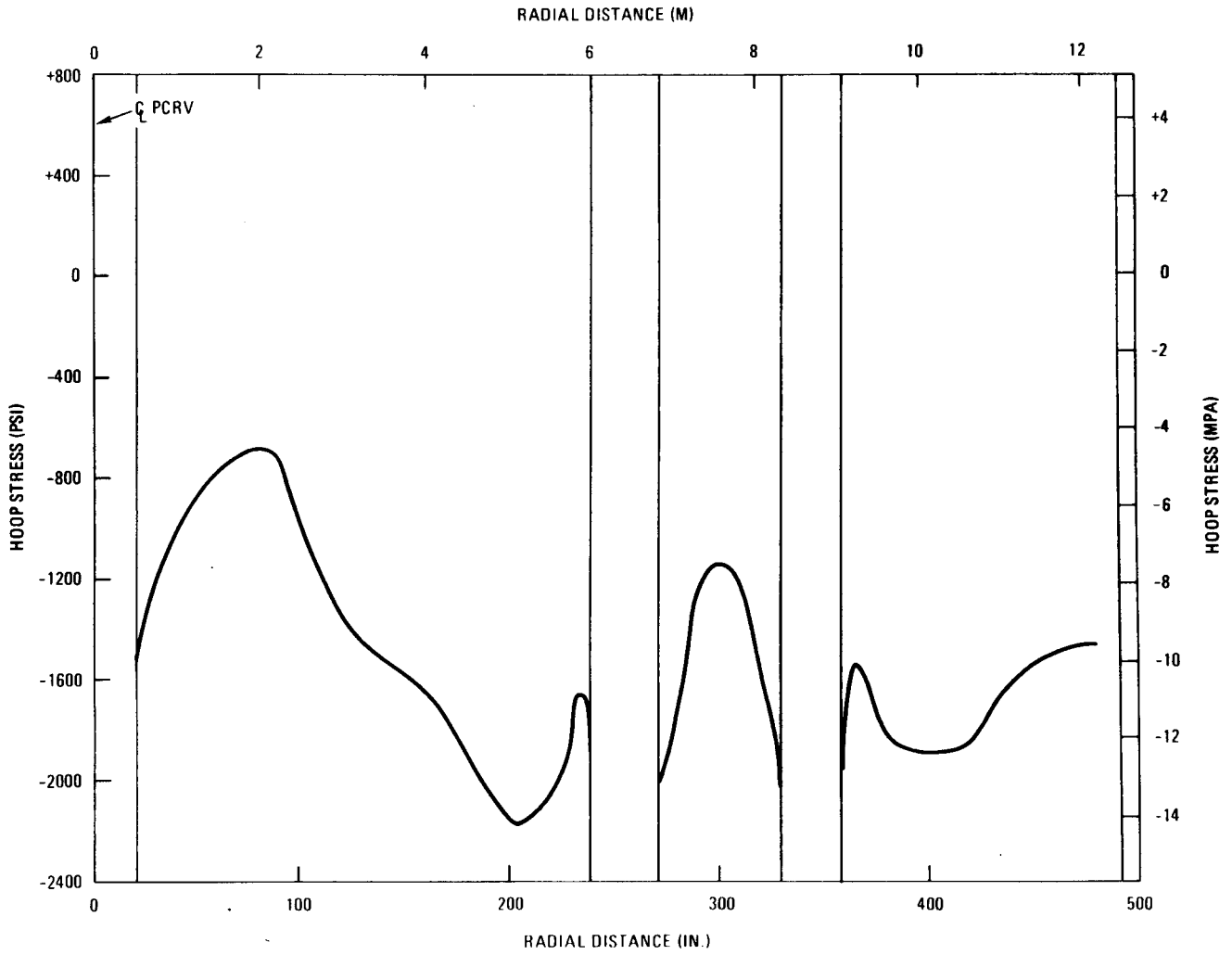

Fig. 37. Hoop stress, section I(E), variable R, Z = 281.75, angle = 0°, loading = F_i

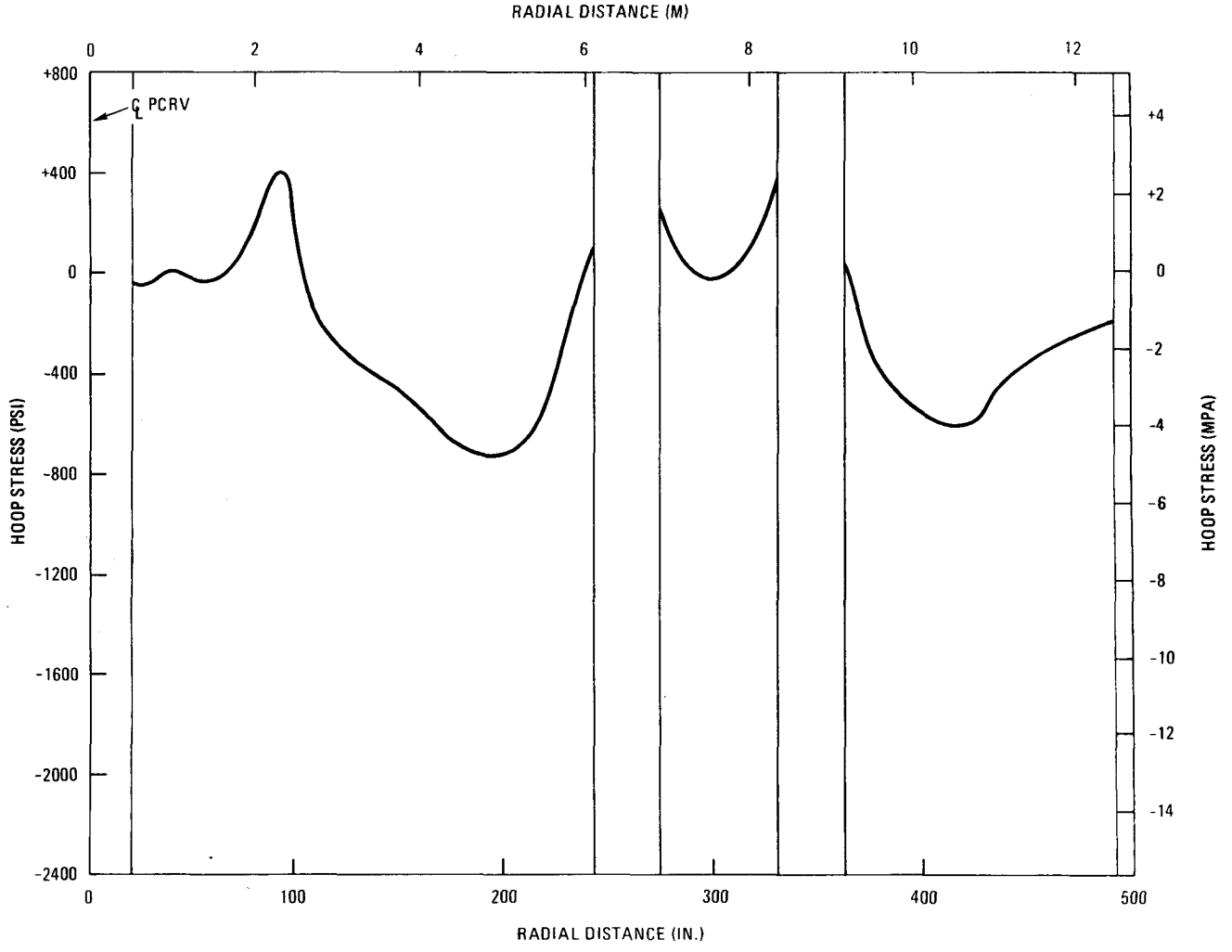

Fig. 38. Hoop stress, section I(E), variable R, Z = 281.75, angle = 0°, loading = F_e + MCP + T_o

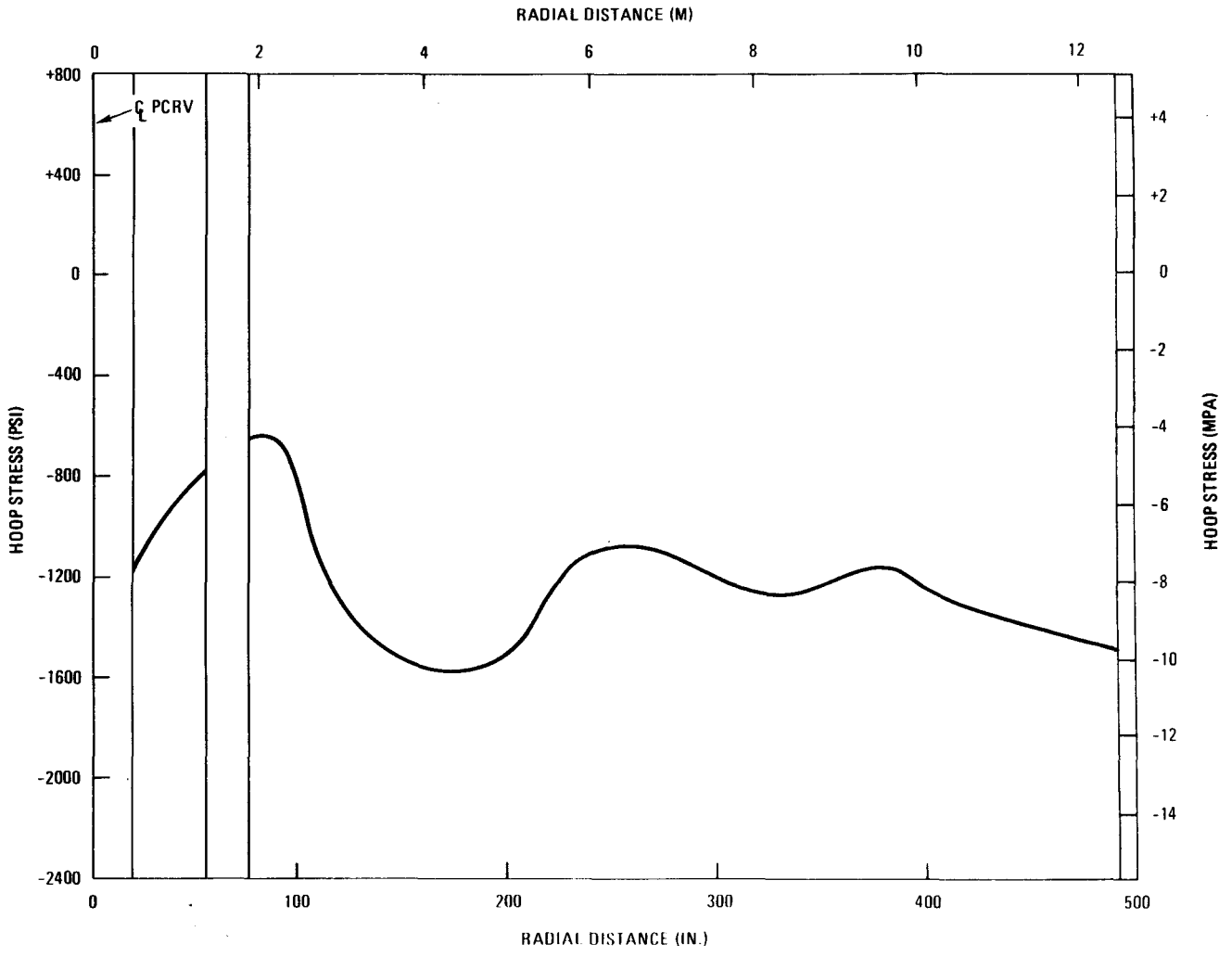

Fig. 39. Hoop stress, section II(E), variable R, Z = 281.75, angle = -60°, loading = F_i

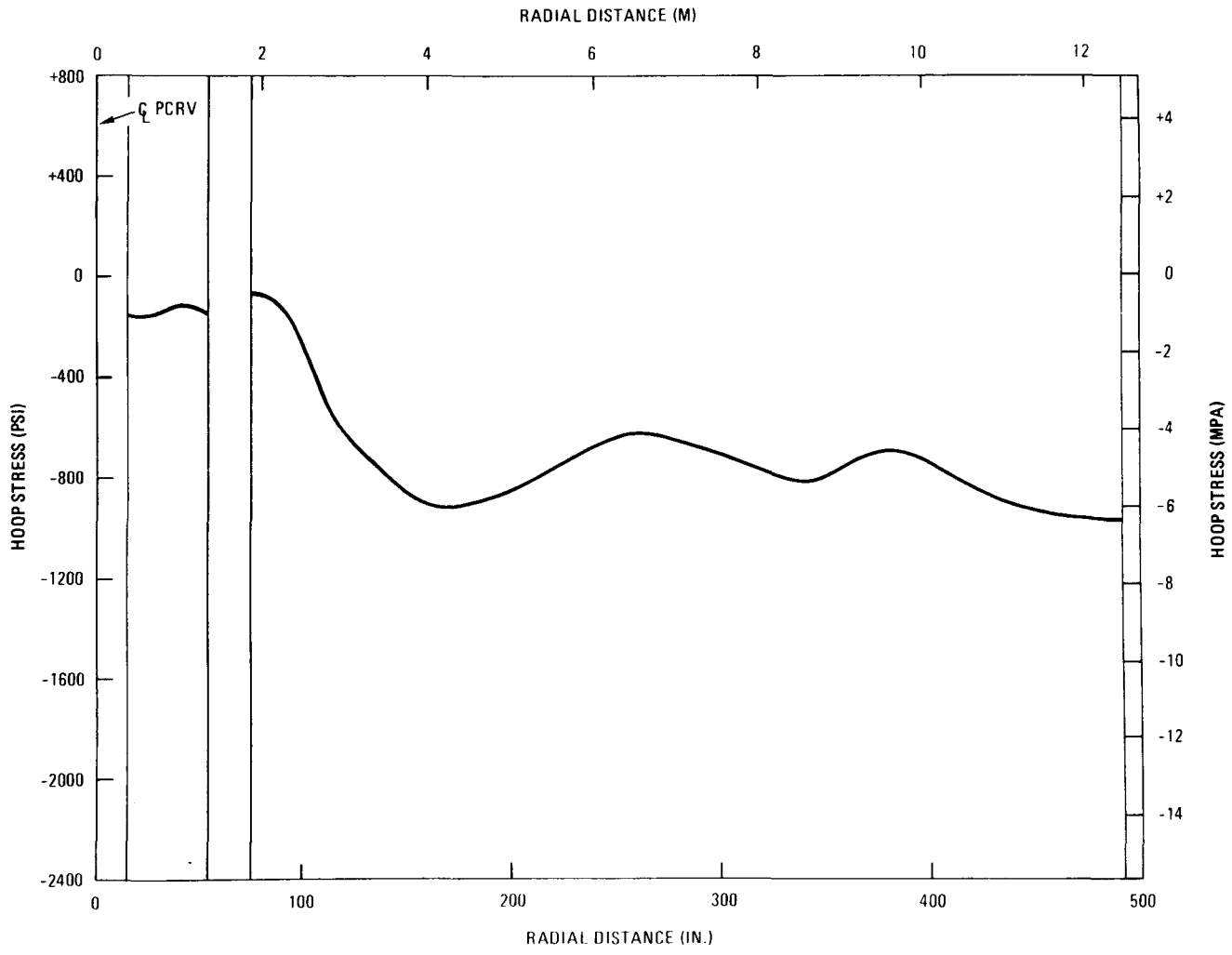

Fig. 40. Hoop stress, section II(E), variable R, Z = 281.75, angle = -60°, loading = F_e + MCP + T_o

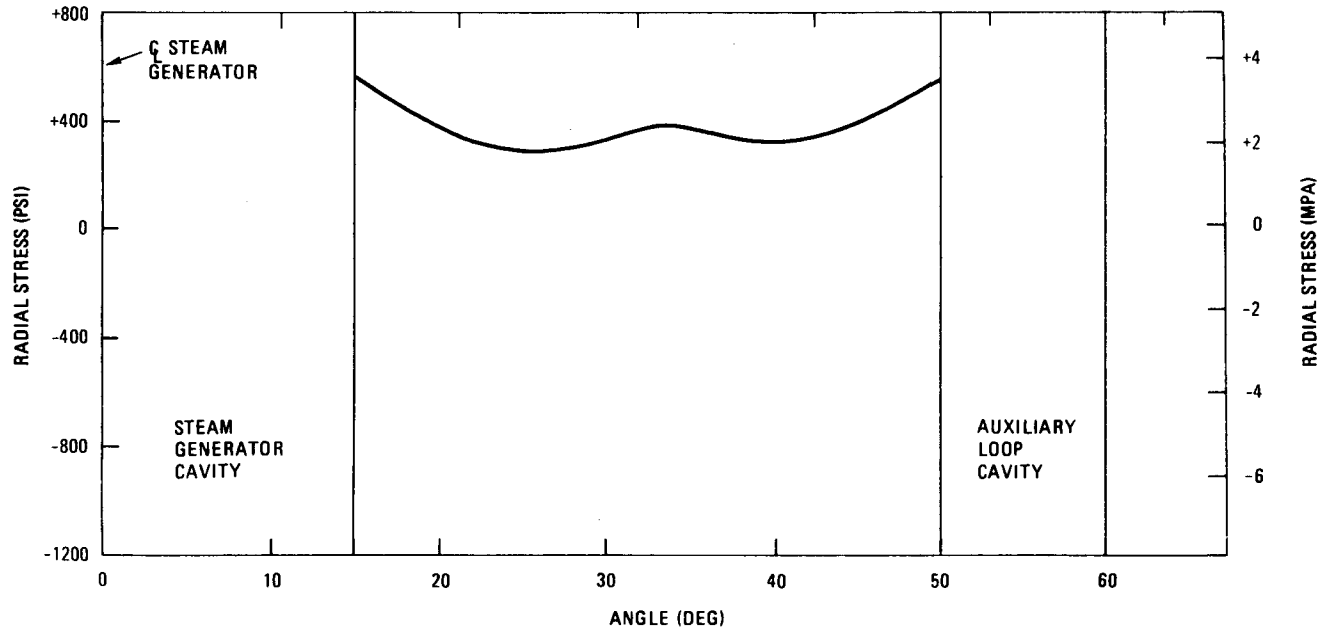

Fig. 41. Radial stress, section IV, R = 267, Z = 1238.8, variable angle, loading = F_i

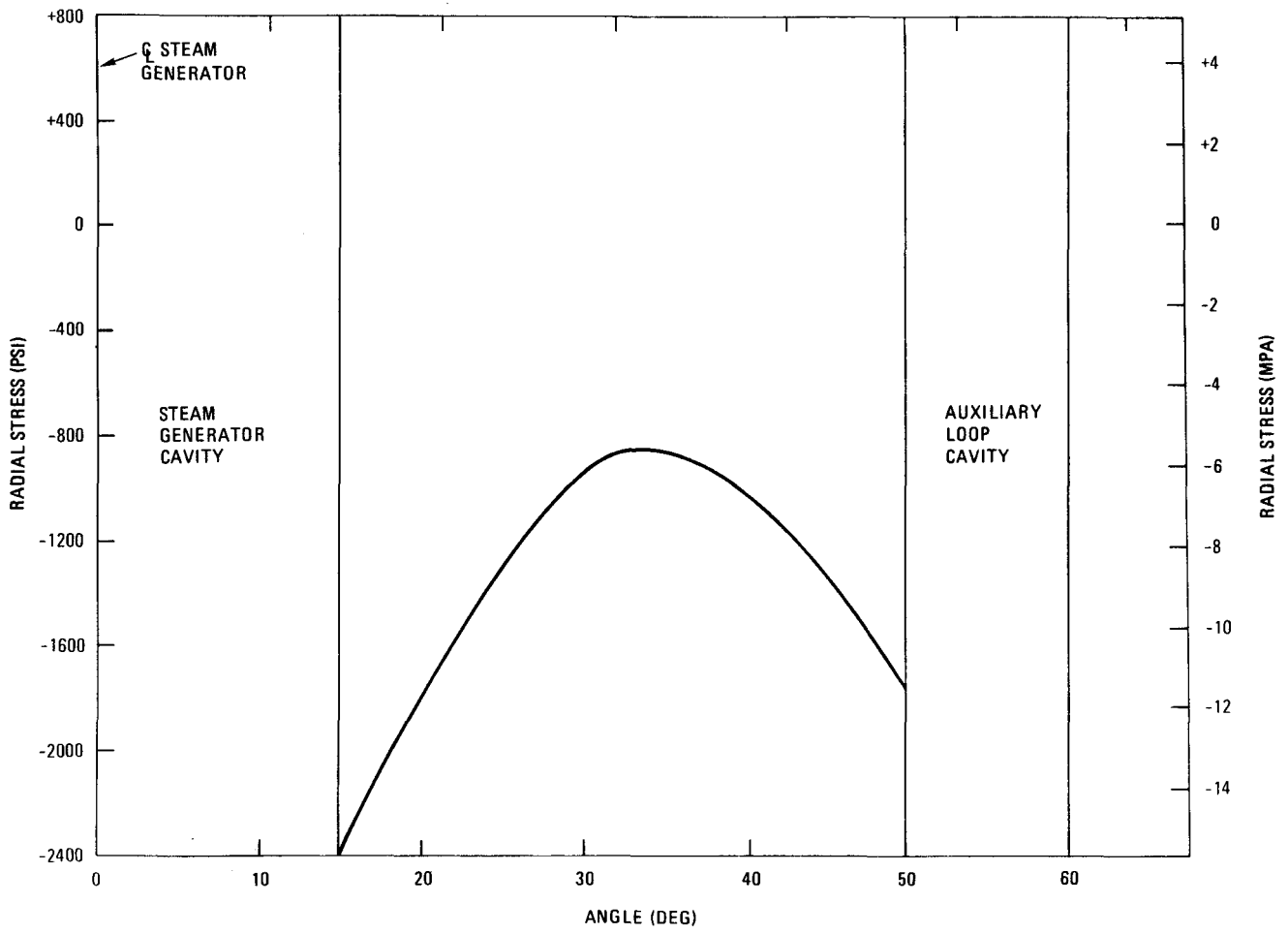

Fig. 42. Radial stress, section IV, R = 267, Z = 1238.8, variable angle, loading = F_e + MCP + T_o